Icarus 380 (2022) 114994

Contents lists available at ScienceDirect

Icarus

journal homepage: www.elsevier.com/locate/icarus

Convective storms in closed cyclones in Jupiter's South Temperate Belt: (I) observations

Ricardo Hueso [a,*], Peio Iñurrigarro [a], Agustín Sánchez-Lavega [a], Clyde R. Foster [b], John H. Rogers [c], Glenn S. Orton [d], Candice Hansen [e], Gerald Eichstädt [f], Inaki Ordonez-Etxeberria [a,g], Jose Felix Rojas [a], Shawn R. Brueshaber [d], Jose Francisco Sanz-Requena [h,i], Santiago Pérez-Hoyos [a], Michael H. Wong [j], Thomas W. Momary [d], Björn Jónsson [k], Arrate Antuñano [a], Kevin H. Baines [d], Emma K. Dahl [d], Shinji Mizumoto [l], Christopher Go [m], Asier Anguiano-Arteaga [a]

[a] Física Aplicada, Escuela de Ingeniería de Bilbao, Universidad del País Vasco UPV/EHU, Plaza Ingeniero Torres Quevedo, 1, 48013 Bilbao, Spain
[b] Astronomical Society of Southern Africa, Centurion, South Africa
[c] British Astronomical Association, Burlington House, Piccadilly, London W1J 0DU, UK
[d] Jet Propulsion Laboratory, California Institute of Technology, 4800 Oak Grove Drive, Pasadena, CA 91109, USA
[e] Planetary Science Institute, 1700 East Fort Lowell, Suite 106, Tucson, AZ 85719-2395, USA
[f] Independent scholar, Stuttgart, Germany
[g] Planetario de Pamplona, 31008 Pamplona, Spain
[h] Departamento de Ciencias Experimentales, Universidad Europea Miguel de Cervantes, Valladolid, Spain,
[i] Departamento de Física Teórica, Atómica y Óptica, Universidad de Valladolid, Valladolid, Spain
[j] Center for Integrative Planetary Science, University of California, Berkeley, CA, USA
[k] Amateur Astronomical Society of Seltjarnarnes, Seltjarnarnes, Iceland
[l] Association of Lunar and Planetary Observers-Japan, Japan
[m] Physics Department-University of San Carlos, Cebu City, Philippines

ARTICLE INFO

Keywords:
Jupiter
Atmospheres
Dynamics

ABSTRACT

On May 31, 2020 a short-lived convective storm appeared in one of the small cyclones of Jupiter's South Temperate Belt (STB) at planetographic latitude 30.8°S. The outbreak was captured by amateur astronomer Clyde Foster in methane-band images, became widely known as Clyde's Spot, and was imaged at very high resolution by the Junocam instrument on board the Juno mission 2.5 days later. Junocam images showed a white two-lobed cyclonic system with high clouds observed in the methane-band at 890 nm. The storm evolved over a few days to become a dark feature that showed turbulence for months, presented oscillations in its drift rate, and slowly expanded, first into a Folded Filamentary Region (FFR), and later into a turbulent segment of the STB over a timescale of one year. On August 7, 2021, a new storm strikingly similar to Clyde's Spot erupted in a cyclone of the STB. The new storm exhibited first a similar transformation into a turbulent dark feature, and later transformed into a dark cyclone fully formed by January 2022. We compare the evolution into a FFR of Clyde's Spot with the formation of a FFR observed by Voyager 2 in 1979 in the South South Temperate Belt (SSTB) after a convective outburst in a cyclone that also developed a two-lobed shape. We also discuss the contemporaneous evolution of an additional cyclone of the STB, which was similar to the one were Clyde's Spot developed. This cyclone did not exhibit visible internal convective activity, and transformed from pale white in 2019, with low contrast with the environment, to dark red in 2020, and thus, was very similar to the outcome of the second storm. This cyclone became bright again in 2021 after interacting with Oval BA. We present observations of these phenomena obtained by amateur astronomers, ground-based telescopes, Hubble Space Telescope and Junocam.

* Corresponding author.
E-mail address: ricardo.hueso@ehu.eus (R. Hueso).

https://doi.org/10.1016/j.icarus.2022.114994
Received 15 November 2021; Received in revised form 14 March 2022; Accepted 15 March 2022
Available online 22 March 2022

This study reveals that short-lived small storms that are active for only a few days can produce complex long-term changes that extend over much larger areas than those initially covered by the storms. In a second paper [Iñurrigarro et al., 2022] we use the EPIC numerical model to simulate these storms and study moist convection in closed cyclones.

1. Introduction

Convective storms on Jupiter appear mostly in regions of cyclonic shear (Little et al., 1999; Ingersoll, 2004; Becker et al., 2020). The exceptions are the convective plumes in the southern anticyclonic side of the North Temperate Belt that give rise to North Temperate Belt Disturbances (Sánchez-Lavega et al., 2017 and references therein). The strongest storms rise into the upper troposphere producing bright outbreaks of clouds that are particularly visible in images in methane absorption bands, where most of the planet is dark, and high-altitude clouds are bright. The methane-bright clouds produced in convective storms can be long-lived in disturbances of the North Temperate Belt (Sánchez-Lavega et al., 2008, 2017) and the South Equatorial Belt (Sánchez-Lavega et al., 1996; Fletcher et al., 2017), where they drive massive changes in the belts' appearance and cloud properties (Pérez-Hoyos et al., 2020). However, in storms developing in other latitudes, the storm activity is much shorter, and the methane-bright clouds dissipate in a few days. Until a few years ago, many of these small-scale storms might have passed unnoticed. However, with the frequent observations of Jupiter motivated by the ongoing Juno mission, and in particular with the contribution of amateur astronomers (Hueso et al., 2018), a very efficient survey of the meteorological activity of the planet is now possible. Thus, the life cycle of small convective storms can be studied in detail.

One of these short-lived storms was discovered by amateur astronomer Clyde Foster on May 31, 2020 and was nicknamed "Clyde's Spot" (Foster et al., 2020). The storm appeared as a bright new small spot in 890 nm images at planetographic latitude −30.8° in the South Temperate Belt (STB). The outbreak occurred in the center of a pre-existing small round cyclone with a diameter of about 2°. This cyclone had very low contrast in visible wavelengths, but it was bright in the UV and dark in methane-bands in HST images acquired weeks before. The storm onset occurred 2.5 days before a scheduled observation of the same area by the Junocam instrument (Hansen et al., 2017), the visible imager on the Juno spacecraft. Ground-based methane-band images obtained in the following days showed a fast decay of brightness. Images in the visible showed the formation of a dark remnant that grew and evolved significantly during 2020 and 2021. This evolution resulted in the formation of a large complex and turbulent cyclonic system with a morphology over most of 2021 similar to Folded Filamentary Regions (FFR), which are features typically found at higher latitudes (Mitchell et al., 1979) and specially abundant at polar latitudes (Orton et al., 2017). The FFR continued to expand longitudinally becoming a turbulent segment of the STB during the last part of 2021.

A very similar storm erupted in the STB on 7 August 2021 in a cyclone with a morphology comparable to the one where Clyde's Spot initiated. The storm was discovered simultaneously by several amateur observers (Tsuyoshi Arakawa, Trevor Barry, Christopher Go and the National Astronomical Research Institute of Thailand) from 890-nm images, and its evolution followed initially a very similar pattern to Clyde's Spot, evolving into a turbulent dark region. However, by January 2022 this feature had transformed into a reddish cyclone, breaking its initial parallelism with Clyde's Spot.

The cyclones where these storms started were only two of several cyclones observable in the STB during 2020–2021. One of them was similar in size to the precursors of both storms and was located at the same latitude. However, it was very dark in all wavelengths in 2020 and was labelled as Dark Spot 6 (DS6) on reports of Jovian atmospheric activity based on amateur data. It was also the first of these three cloud systems that was noticd in ground-based observations of Jupiter. Reddish dark cyclones are uncommon features in the STB and have been observed occasionally at those latitudes (Rogers et al., 2013; Simon et al., 2015). While this cyclone never showed internal convective activity, it experienced remarkable changes in its morphology, size and colour, changing from a low-contrast white cyclone in 2019, to a dark aspect in 2020, and appearing as a bright cyclone after solar conjunction in January 2021.

The typical circulation in a cyclone in the south hemisphere is clockwise rotation with downwelling in the interior and upwelling along the edges. This basic circulation explains why most cyclones are dark in methane-band images and sometimes have bright rings of material around them, including active convection in their edges (see for instance the elongated ammonia plume around an elongated cyclone in Fig. 3 in Reuter et al., 2007). Both Clyde's Spot and the 2021 STB storm were convective outbreaks that developed inside closed cyclones, and not in their edges. In both cases, the interaction between the circulation of the original cyclones and the expanding motions of the storms confined the bright clouds forming a characteristic double-lobed structure in the 2–3 days after convection started. This is a very similar behavior to one of the convective storms observed during the Voyager 2 flyby in 1979 (Smith et al., 1979). Voyager 2 observed a cyclone in the South South Temperate Belt (SSTB) that developed a convective storm that formed a double-lobed cloud system that quickly evolved to form a FFR.[1] Interestingly, the two storms in the STB studied in this paper were very different to the set of convective outbreaks that occurred inside an elongated cyclone of the STB in 2018 (Iñurrigarro et al., 2020) at nearly the same latitude as the 2020 and 2021 events.

Here we present an observational analysis of these three meteorological systems combining amateur images, ground-based observations, HST and Junocam data. As a guide to the rest of this paper, Fig. 1 shows a summary of the different morphologies of the evolution of Clyde's Spot. Fig. 2 shows snapshots of the temporal evolution of the storm that developed one year later. Fig. 3 shows the different morphologies of the apparently non-convective cyclone DS6.

The goal of this manuscript is to document the evolution of these actively convective cyclones and provide observational details to investigate the relationship between cyclonic shear and moist convection (Dowling, 1995; Thomson and McIntyre, 2016; Fletcher et al., 2017; Iñurrigarro et al., 2020). In order to compare Clyde's Spot and the 2021 STB storm with similar convective events in closed cyclones, we perform a reanalysis of the Voyager 2 observations of the 1979 storm in the SSTB. In a companion paper [Iñurrigarro et al., 2022, hereafter paper 2], we present numerical simulations of Clyde's Spot, the 2021 STB storm, and the Voyager SSTB storm using the Explicit Planetary Isentropic-Coordinate model (EPIC) (Dowling et al., 1998). We also compare the results of those simulations with similar EPIC simulations of the convective storm that developed in an elongated cyclone of the STB in 2018 (Iñurrigarro et al., 2020). In particular, we show in paper 2 that the structure of the double-lobed morphology observed in Clyde's Spot (Fig. 1c), the 2021 STB storm and the 1979 SSTB storm is due to the interaction of the cyclonic circulation in the vortex and the central convective pulse.

The structure of this paper is as follows. Section 2 summarizes the observations. Section 3 presents the outbreak of Clyde's Spot. Section 4

[1] A movie of this convective storm is available on NASA's photojournal at https://photojournal.jpl.nasa.gov/catalog/PIA02257

discusses the origin of this feature and the DS6 cyclone in 2019 and their mid-term evolution over 2020. Their evolution over 2021 is presented in Section 5. Section 6 shows the August 2021 STB storm. In Section 7 we compare both recent STB storms with the storm in one cyclone of the SSTB observed by Voyager 2. We discuss our results in Section 8 and present our conclusions in Section 9. Unless otherwise expressed, all longitudes are given in System III, and all latitudes are planetographic.

2. Observations

2.1. Amateur observations

There are many amateur astronomers involved in the global campaign in support of the Juno mission (Fletcher and Rogers, 2018). Most of their observations can be downloaded from the PVOL database (http://pvol2.ehu.eus/; Hueso et al., 2018) or ALPO Japan image repository (http://alpo-j.sakura.ne.jp/indexE.htm). These images are obtained with telescopes with apertures in the 20–50 cm range, fast cameras acquiring video observations of the planet, and image stacking and processing software resulting in high-resolution images (Mousis et al., 2014). About 550 images from more than 50 observers have been used in this work. Table 1 presents a list of the key observers.

2.2. PlanetCam UPV/EHU

The PlanetCam UPV/EHU instrument is a dual-channel high-resolution lucky-imaging instrument that observes from 380 nm to 1.7 μm using two cameras that operate in parallel in the visible (380–1000 nm) and in the short-wave infrared (1.0–1.7 μm). Mendikoa et al. (2016) describe the instrument in detail. Each camera is equipped with broad and narrow-band filters and the instrument operates in either the 1.2 m or the 2.2 m telescopes at Calar Alto observatory. We run a long-term survey of atmospheric activity in Jupiter with at least 2 observing runs of 4 nights per year. We use the lucky-imaging method with fast acquisitions and stacking of the best frames. Although, in principle, the stacked images can be calibrated and used for radiative transfer modeling, the small size of the cyclones studied here does not allow for adequate separation of their properties from the surrounding regions. Thus, we will only present high-pass versions of the images, discussing the morphology of the features in the observations and their visibility in filters that sample different levels of the atmosphere. PlanetCam observations are summarized in Table 2.

2.3. Thermal infrared images: NASA IRTF and Gemini

We also examined 5.1 μm images of Jupiter obtained at IRTF in the period from 2019 to 2021 using the scientific-grade guide camera ("GuideDog") of the moderate-resolution SpeX near-infrared spectrometer (Rayner et al., 2003). These images were used to explore possible changes in the cloud opacity at depth of the cyclone where the storm developed and in other STB cyclones. The observations examined represent only a small part of the much larger set of IRTF observations of Jupiter acquired from 2019 to 2021. We also present one map at 4.7 μm taken with the NIRI instrument at the Gemini North observatory, with spatial resolution optimized using a lucky imaging approach. This Gemini map is part of the imaging program described in Wong et al., (2020). Table 2 summarizes these observations.

2.4. Hubble space telescope

We have examined HST Wide Field Camera 3 images of Jupiter acquired from 2019 to 2021, which we retrieved from the Mikulski archive for space telescopes (https://archive.stsci.edu/). These images were used to track the features of interest, examine their morphology, and obtain winds in the Clyde's Spot Remnant months after the convective outbreak. Specific dates and details are given in Table 2.

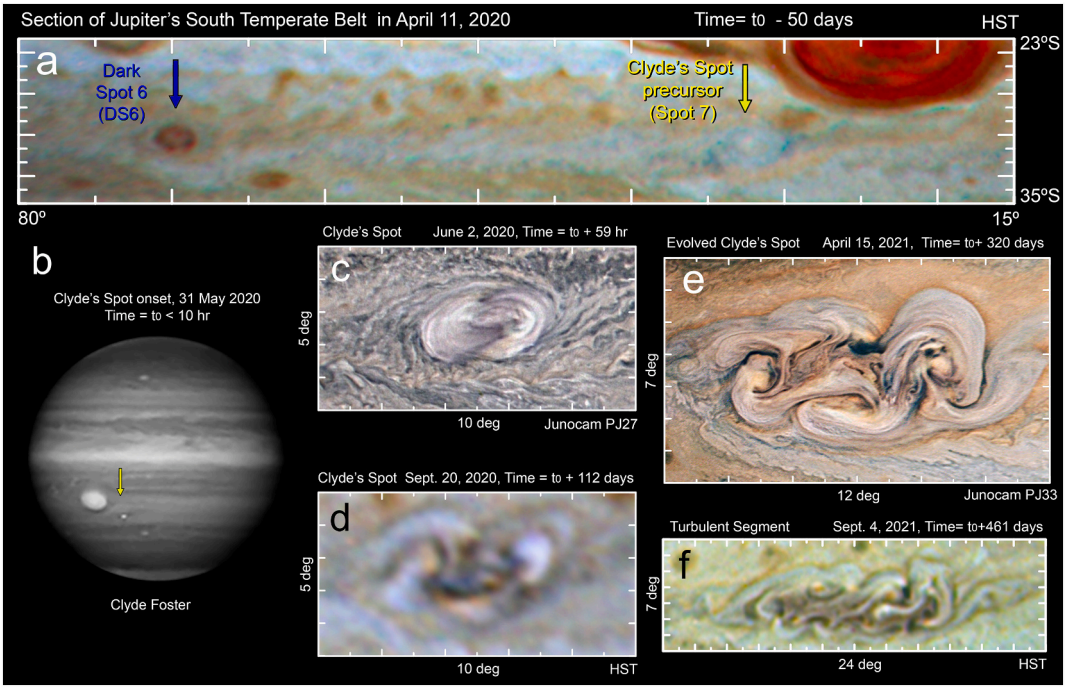

Fig. 1. Clyde's Spot and its evolution over 2020 and 2021. (a) Section of the STB in April 2020 showing two distinct cyclones: Dark Spot 6 (DS6), and a low-contrast bright cyclone close to the GRS that was the precursor of Clyde's Spot. System III longitudes and planetographic latitudes are given. (b) Methane-band discovery image showing the convective eruption on Clyde's Spot. (c) Junocam image of Clyde's Spot. (d) HST observation of Clyde's Spot Remnant. (e) Fully developed FFR on Clyde's Spot nearly one year after the convective eruption. (f) Longitudinal expansion of the FFR into a turbulent segment of the STB. Numbers outside individual panels indicate the longitudinal and latitudinal domains shown. Panels c, d, and e are shown at the same scale.

2.5. Junocam

Junocam is a wide-angle camera onboard the Juno spacecraft. Images are obtained at the perijoves in Juno's highly elliptical orbit of 53-days. The detector is masked with broadband filters in red, green and blue, as well as in the methane band at 890 nm. Colour images are obtained by observing the same region of the planet with the different filter strips while Juno moves and rotates. Junocam images are not photometrically calibrated. The spatial resolution of the observations can reach 3 km/pixel over the equator when observed at the perijove, and is about 50 km/pixel over the poles (Hansen et al., 2017). Because of the wide-angle view obtained from a close proximity, and the time it takes to obtain an image while the spacecraft rotates, the effective resolution of the observations varies in different locations of each image. Because of the fast trajectory of the spacecraft and short distance to the planet during the perijoves, the ability to obtain repeated observations of the same area at low latitudes is limited. For the mid and low latitudes, images of the same area can be obtained with typical time separations of 10 min. Table 3 lists the Junocam observations used in this work. Images from Perijove 27 (PJ27) are explained in greater detail because they were used for a detailed analysis of cloud motions.

3. Clyde's Spot convective outbreak

3.1. Initial observations: amateur and HST

A bright and compact cloud feature appeared in a methane band image at 890 nm acquired by Clyde Foster on 31 May 2020 at 00:34UT (Foster et al., 2020) (Fig. 4b). Observations in RGB and IR filters showed the same compact bright cloud immersed in a slightly dark elongated segment of the STB (Fig. 4d). Methane band observations obtained one Jupiter rotation earlier by another observer, Andrew Casely, did not show the same feature (Fig. 4a).

An examination of amateur images over March–April 2020 (Supplementary Fig. S1) shows that Clyde's Spot had erupted in a preexisting cyclone with a very low contrast in images in the visible (Fig. 1a), but bright in HST UV images. This UV bright aspect is similar to cyclonic vortices in the South Equatorial Belt precursors of convective outbreaks in early 2017 (de Pater et al., 2019). Additional observations over 2019 and early 2020 show that this particular cyclone, as well as DS6, were the outcome of mergers of smaller cyclones in the STB (Supplementary Text S1, and Supplementary Figs. S2 and S3).

The compact structure of Clyde's Spot, its rapid development, and its intense brightness in all wavelengths, especially in the methane band, all suggest the onset of a convective storm captured in the first hours of its development. Methane band images obtained 20 h later showed the same bright compact cloud with a slightly larger size but apparently lower brightness (Fig. 4c), suggesting continuous convection, but at a smaller rate after an initial strong outbreak.

The original amateur methane-band discovery images of Clyde's Spot were examined using a simple Reflective Layer Model (RLM) (e.g. Mendikoa et al., 2012) to get a first order estimate of the altitude of the cloud tops on the storm with respect to their surroundings. For this purpose, we examined the original stacks of frames before applying any image enhancement filter. The RLM fits the observed reflectivities along a latitude circle considering the methane absorption coefficient (which can be computed from the transmission function of the filter), the scattering angles at each position, and two cloud parameters: the pressure at the top of the cloud and the reflection coefficient. Because these observations could not be calibrated with a reference star, only the relative photometry of features in Jupiter can be examined. A photometric cut at the latitude of the storm shows that Clyde's spot is at least 7% brighter than its environment. Model fitting suggests that the bright clouds are located ~0.25–0.30 scale heights above their environment (i.e. 4–5 km). However, this must be taken as a lower limit to the cloud altitude. The small size of the storm (~0.7 arcsec), combined with the atmospheric seeing and diffraction limit (~0.6 arcsec at 890 nm for the 14 in. telescope used), mean that the storm could have been smaller and brighter, which would have resulted in higher cloud tops. Further analysis of observations in visible wavelengths was unsuccessful due to the low contrast of the feature in the unprocessed photometric images.

HST observations in support of Juno were acquired 48.8 h after the initial observation. These images were obtained with the storm rising very close to the limb of the planet, limiting their capability to provide accurate data for a radiative transfer calculation. Fig. 5 shows maps of Jupiter from a selection of HST images. UV and blue images show the bright clouds of the storm. The storm is also bright and highly contrasted at 890 nm. Green and red wavelengths show Clyde's Spot as a darker structure than its environment with some small bright inner cores with sizes of about 300–600 km. The largest bright core inside Clyde's Spot,

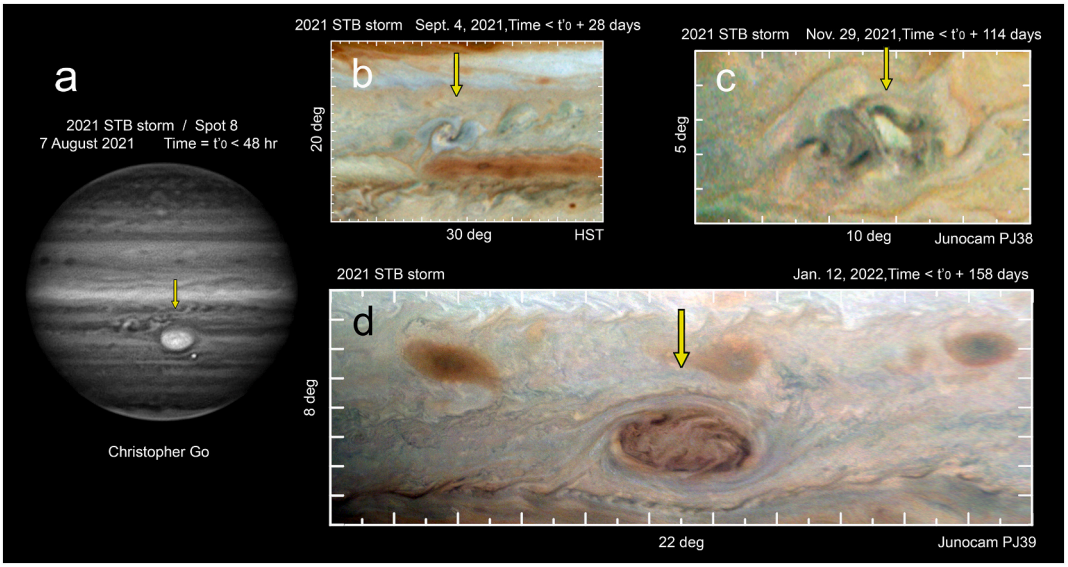

Fig. 2. The 2021 STB storm and its evolution. (a) Methane-band image of the convective outbreak in August 2021. (b) HST image of the storm one month later. (c) Junocam observation obtained in November 2021. (d) Junocam observation in January 2022. Numbers outside individual panels indicate the longitudinal and latitudinal domains shown. Panels c, and d are shown at the same scale.

highlighted with a yellow-orange arrow in Fig. 5, is visible in all filters, except in the 727-nm and 890-nm weak and strong methane-bands, where it is not a distinguishable feature inside the bright storm. Thus, the individual bright cores are probably deeper than the overall cloud system, and their high brightness in UV and visible wavelengths may reflect compact clouds with large cloud opacity.

3.2. Junocam images: morphology and wind field

Junocam observed the storm 10 h after HST and 59 h after the images of its explosive onset. Fig. 6 shows Junocam maps in the visible and methane band. Fig. 6a presents the same exact region as Fig. 5, so that both scenes can be directly compared. The storm's shape is that of an elongated cyclone, tilted with respect to the zonal direction and with a largest diameter of 4600 ± 300 km and a shortest of 2700 ± 200 km. Its latitudinal location is on the cyclonic side of the local westward jet, inside a larger elongated structure with spiral arms visible in the colour image. The zonal-wind profile shown in Fig. 6a is the one measured from HST images in 2016 by Hueso et al. (2017) updated with further amateur and HST data from 2017. Fig. 6b shows a highly magnified version of the storm using the visible and methane-band maps, multiplying both images and contrasting the result, so that the brightest and highest regions can be highlighted. Compact features visible in these images have characteristic sizes that range from 200 to 850 km. These sites possibly represent the locations of recent active convection forming elevated "anvil" clouds. Fig. 6c and d show versions of the storm in visible wavelengths and in the methane band respectively at an intermediate resolution, so that the details of the storm and its environment can be examined.

A comparison of the HST image on Fig. 5b and the Junocam image on Fig. 6c shows that the bright cores highlighted with arrows in Fig. 5b may have counterparts in the brightest areas of the Junocam image indicated with arrows in Fig. 6c. If these features are the same, this comparison would result in a storm-wide cyclonic circulation pattern with 30–35 ms^{-1} velocities at distances to the vortex center of 1500 ± 450 km. A rough measurement of the mean vorticity of the cyclone can be obtained from using the circulation theorem:

Table 1
Key amateur contributors to this study.

Oberver	Number of images used	Filters	Period
T. Barry	30	RGB, IR, CH4	March 2019 – Sept. 2021
A. Casely	27	RGB, IR, CH4	Feb. 2019 – Nov. 2021
J. L. Dauvergne	15	RGB	June 2019 – Nov. 2021
C. Foster	115	RGB, IR, CH4	March 2019 – Dec. 2021
C. Go	74	RGB, IR, CH4	April 2019 – Nov. 2021
N. MacNeill	28	RGB, IR	Oct. 2019 – Oct. 2021
P. Miles	5	RGB, IR	Aug. 2020 – Oct. 2020
T. Olivetti	26	RGB, IR	Feb. 2019 – Dec. 2021
D. Peach	11	RGB	Aug. 2019 – Oct. 2021
E. Sussenbach	17	RGB	Feb. 2020 – August 2021
A. Wesley	54	RGB, IR, CH4	Apr. 2019 – June 2021

Notes: IR in the table indicates different long-pass filters generally producing high-resolution observations of the planet at wavelengths shorter than 1 μm. CH4 refers to narrow-band filters centered at the 890 nm methane absorption band.

$$\oint \vec{v}\cdot d\vec{r} \approx \int \xi ds \tag{1}$$

where v is the velocity in the periphery of the cyclone at distance r from the center of the vortex and ξ is the vertical component of the vorticity integrated over the area s of the cyclone. Thus, the overall vorticity $\xi \approx 2v/r$ can be estimated as $(-4.9 \pm 1.7)\text{x}10^{-5}$ s^{-1}.

A better measurement of velocities can be obtained from the PJ27 Junocam images described in Table 3. We mapped those images in cylindrical projections and measured the apparent motions of the clouds. However, any small error in the navigation of images results in small distortions in the projected maps, and because of the small time difference between images (~10 min), a wind correction technique is needed

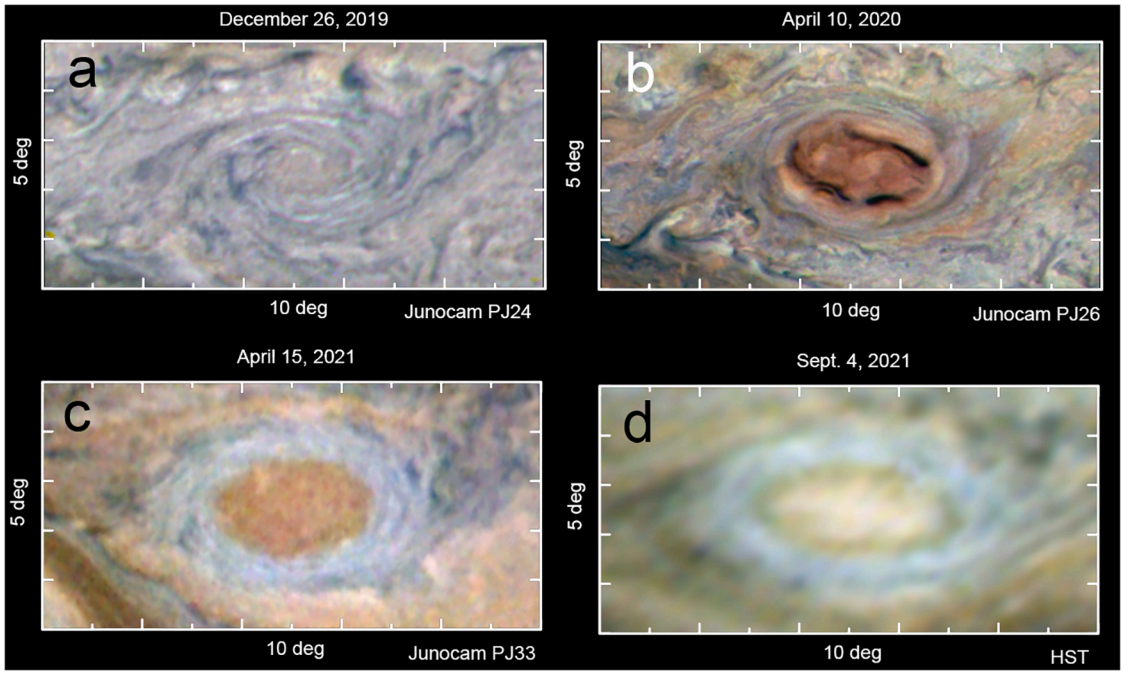

Fig. 3. Dark Spot 6 (DS6). Different views of the non-convective cyclone DS6 over 2019–2021. Panels are centered at 30.5° S. Numbers outside individual panels indicate the longitudinal and latitudinal domains shown. Note the bright rings around the cyclone in panels b-d consistent with updraft in the edges of the cyclone.

Table 2
Observations on different facilities.

Source	Dates (yyyy-mm-dd)	Observing program ID	Used for	PI of the observations
HST / WFC3	2019-02-12	14,661	T	M.H. Wong
	2019-04-06	15,665	T	I. de Pater
	2019-04-07		T	
	2019-04-08		T	
	2019-04-09	15,159	T	M. H. Wong
	2019-06-27	15,502	T	A. Simon
	2019-09-12	14,661	T	M.H. Wong
	2020-04-11	16,074	T	M.H. Wong
	2020-06-02		T, M	
	2020-07-23	16,053	T, M	I. de Pater
	2020-07-24		T, M	
	2020-08-25	15,929	T, M	A. Simon
	2020-09-20		T, M, W	
	2021-09-04	16,266	M	
IRTF	2019-11-05	2019B069	M	G. S. Orton
	2020-08-16	2020B023	M	
	2020-10-04	2020B023	M	
	2021-04-13	2020B041	M	
	2021-06-07		M	
	2021-07-21		M	
	2021-07-22		M	
Gemini North	2021-06-07	GN-2020B-Q-101	M	M.H. Wong
PlanetCam/ 2.2 m	2019-07-18	2019B-2.2-14	T, M	A. Sánchez-Lavega
	2019-07-20		T, M	
PlanetCam/ 1.2 m	2020-08-08	–	T	
PlanetCam/ 2.2 m	2020-10-31	2020B-2.2-06	T, M	
	2021-06-07	2021A-2.2-09	T, M	P. Iñurrigarro
	2021-07-20	2021B-2.2-010	T, M	A. Antuñano
	2021-07-21			

Note: T stands for Tracking, M stands for Morphology and W stands for Winds.

Table 3
Junocam observations used in this work.

Perijove	Date	Usage	
PJ 19	2019-04-06	T, M	
PJ 20	2019-05-29	T, M	
PJ 24	2019-12-26	T, M	
PJ 26	2020-04-10	T, M	
PJ 27	2020-06-02	M, Winds	
PJ 27 Image	Date & Time	Image pair	Best resolution (km)
JNCR_2020154_27C00040	2020–06-02T10:52:57		25.7
JNCR_2020154_27M00041	2020–06-02T10:54:27	(*)	–
JNCR_2020154_27C00042	2020–06-02T10:56:58	1	30.3
JNCR_2020154_27M00043	2020–06-02T10:58:28	(*)	–
JNCR_2020154_27M00044	2020–06-02T10:59:58	(*)	–
JNCR_2020154_27C00045	2020–06-02T11:01:59	2	36.3
JNCR_2020154_27M00046	2020–06-02T11:03:30	(*)	–
JNCR_2020154_27C00047	2020–06-02T11:07:01	1	42.2
JNCR_2020154_27C00048	2020–06-02T11:13:02	2	49.5
JNCR_2020154_27C00049	2020–06-02T11:19:03		56.7
JNCR_2020154_27C00050	2020–06-02T11:25:05		63.8
Perijove	Date	Usage	
PJ 28	2020-07-25	T, M	
PJ 29	2020-09-16	T, M	
PJ 30	2020-11-08	T, M	
PJ 31	2020-12-30	T, M	
PJ 33	2021-04-16	T, M	
PJ 34	2021-06-08	T, M	
PJ 35	2021-07-21	T	
PJ 38	2021-11-29	M	
PJ 39	2022-01-12	M	

Note: T stands for Tracking, M stands for Morphology. Perijoves 19 to 27 were used to look for cyclones in the STB. Perijoves 29 to 31 were used to look for possible cyclone candidates for the August 2021 storm. Image pairs are identified with a number and methane band images with (*). Resolution corresponds to the pixel scale at the subspacecraft point. The effective resolution of Junocam methane band images is significantly worse than the pixel size due to image noise.

to retrieve cloud motions. We used the following procedure similar to the one used by Sánchez-Lavega et al. (2018): (1) We measured the apparent motions of features outside the convective storm in a region around the storm (shadowed area in Fig. 6a); motions in that region are expected to follow the zonal winds. (2) We compared our measurements in that calibration area with the known zonal winds (Hueso et al., 2017) and used the differences to compute an empirical wind correction model that corrects the effects of image distortions in the winds. (3) We measured the apparent cloud motions in the region inside the calibration area and applied the correction model.

The wind measurements were obtained on two image pairs (see Table 3) using a cloud correlation software called PICV (Particle Image Correlation Velocimetry; Hueso et al., 2009) that measures displacements with sub-pixel accuracy by modeling the correlation map of each individual measurement. Formal errors in the retrievals of the winds from the displacement of one single pixel over the time span of both images result in 78 and 75 ms^{-1} for the first and second image pairs, respectively. However, tests on synthetic images and HST images indicate that an improvement better than a 0.5 pix displacement is possible in regions with contrasted features, and the statistics of motions in nearby locations can be used to reduce the overall errors. Each image pair was navigated and mapped with different approaches, although both sharing the same geometric information derived from SPICE kernels of the mission. One image pair (pair 1 in Table 3) was navigated and processed as described in Sánchez-Lavega et al. (2018). The second image pair (pair 2 in Table 3) was navigated and mapped using the ISIS software as described in Barrado-Izagirre et al. (2021). We obtained one correction model for each image pair. The size of the interrogation window (or correlation box) used for correlation varied from 0.3 × 0.3° at the storm's core to 1.5°x1.5° in the outer parts of the region measured. In general, small interrogation windows can be used in regions with high contrast, and large interrogation windows are needed in regions of low contrast (Hueso et al., 2009). Measurements were visually inspected one-by-one, examining the tracer identified by the software in the original image, its proposed match in the second image, the two-dimensional correlation map, and the corresponding wind vector, so that obvious mistakes in the correlation could be identified and eliminated.

We obtained a dense mesh of corrected measurements in each image pair (2460 wind measurements for the first image pair and 3112 wind measurements for the second image pair). We combined results from both image pairs interpolating the winds in a continuous map of zonal and meridional winds with a resolution of 0.015° and averaging results from both sets of winds. The wind values were then smoothed using a spatial resolution of 1.0° that smooths the effect of local outliers. The result of this combined analysis is shown in Fig. 7, but we note that very similar global motions and vorticity fields were found on each individual image pair.

There are some caveats in this procedure: Firstly, while the motions of large features are well resolved, the motion of small features, such as those present in Fig. 6c, are difficult to measure, and local outliers are

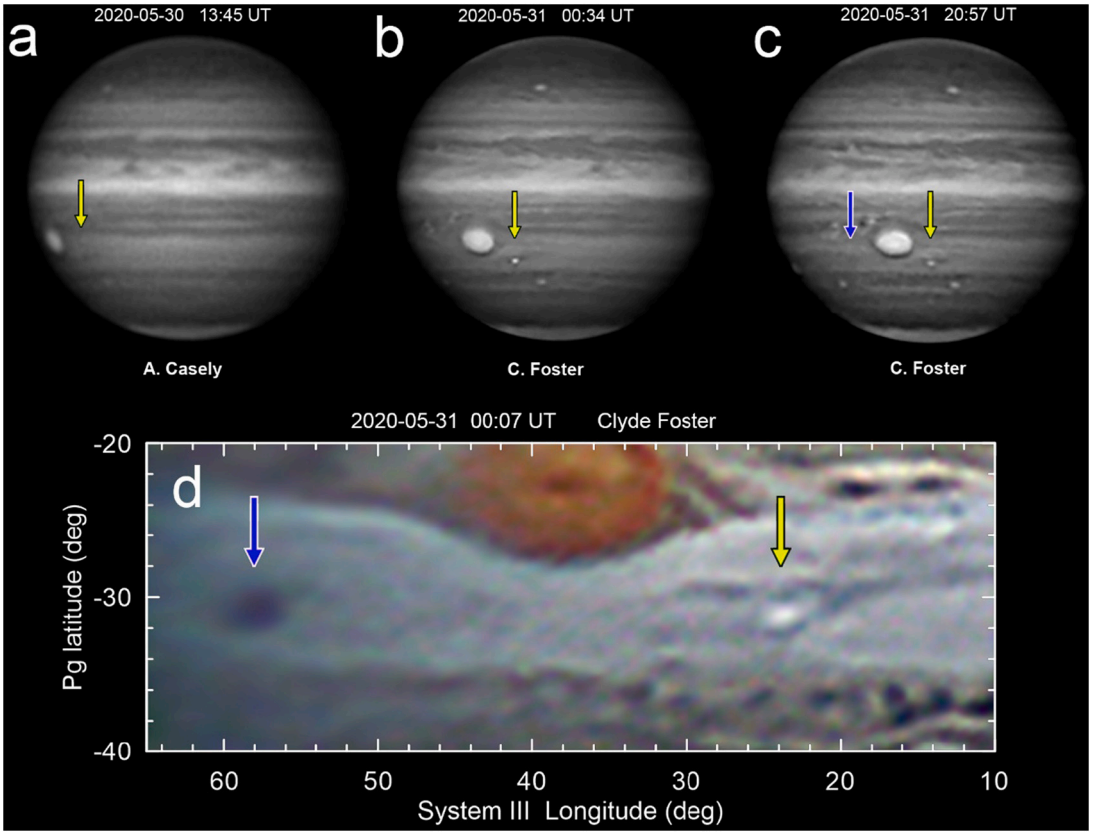

Fig. 4. Onset of the convective storm. (a-c) Series of methane band images at 890 nm acquired on 30 and 31 May 2020. (d) Combination of high-pass filtered observations in visible and IR wavelengths to show the storm at its onset. Individual observers for these images are A. Casely for the 30 May image and C. Foster for all others. Yellow arrows highlight the convective storm. Blue arrows indicate DS6, which was invisible in methane band images. (For interpretation of the references to colour in this figure legend, the reader is referred to the web version of this article.)

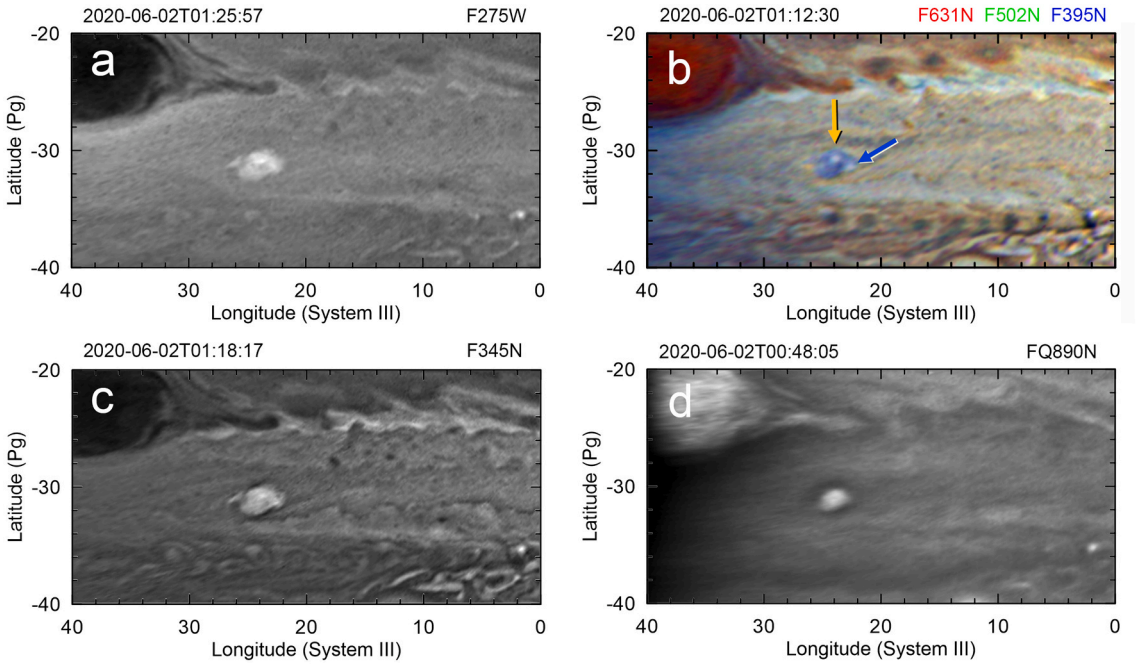

Fig. 5. HST observations of Clyde's Spot 49 h after its onset. Colored arrows in the top right panel indicate two bright compact features inside Clyde's Spot. The methane-band image at 890-nm was acquired with the storm 70° away from the central meridian.

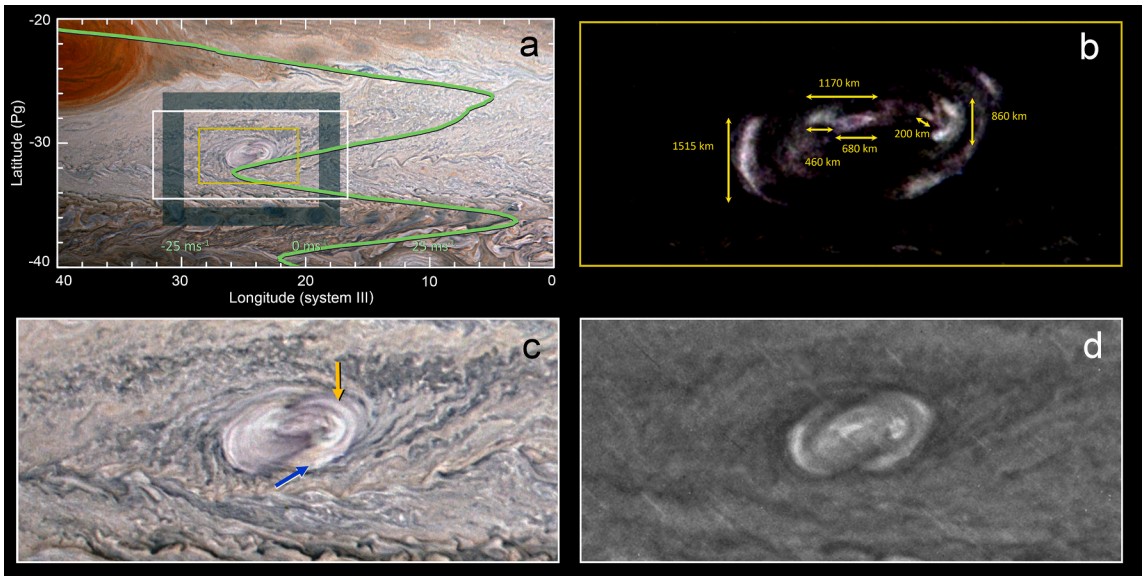

Fig. 6. Junocam observations of the convective storm. (a) Context image showing the region observed by HST 10 h earlier displayed in Fig. 5. The green line is a plot of the zonal winds from −50 to +50 ms^{-1} from Hueso et al. (2017). The yellow box highlights the region shown at higher resolution in panel (b) and the white box marks the regions shown in panels (c) and (d) in colour and at 890 nm respectively. The dark shadowed area shows the region used to calibrate image distortions and correct wind measurements (see text). (b) Highly contrasted zoomed map of the storm obtained from multiplying the visible and methane band images. (c) Zoomed version of the colour image. Colored arrows show candidates to bright features observed in HST 10 h before. A cyan line shows the scale of features in this image. (d) Zoomed version of the methane-band image. All the images have been high-pass processed to increase the visibility of faint details. (For interpretation of the references to colour in this figure legend, the reader is referred to the web version of this article.)

unavoidable. Secondly, the smoothing can artificially decrease narrow and intense circulations. Thus, our results are only pertinent to the mean storm-wide motions. With these caveats the results from this analysis indicates a storm-wide circulation of about 30–40 ms^{-1} with a mean cyclonic vorticity of $(-3.0 \pm 0.8)x10^{-5}$ s^{-1} computed from the circulation theorem. However, the vorticity is concentrated in a ring around the storm where vorticity can reach values of $(-3.5 \pm 0.5)x10^{-5}$ s^{-1} (Fig. 7). These results are roughly compatible with the vorticity obtained from a direct comparison of HST and Junocam images obtained above, $(-4.9 \pm 1.7)x10^{-5}$ s^{-1}. These estimations of the vorticity in the storm are larger than the local vorticity from the meridional shear of the zonal winds, which is $-du/dy = -1.19 \times 10^{-5}$ s^{-1}, and much smaller than the local planetary vorticity $f = -1.8 \times 10^{-4}$ s^{-1}. Our analysis cannot resolve expansion motions of possible intense dynamics in small regions inside the storm.

3.3. Growth rate of the storm

We measured the mean size of the storm in a combination of amateur, HST and Junocam images to investigate the initial expansion and growth of the storm. Amateur images were selected using only those in the methane band or those in IR filters where the storm appeared as a compact well-defined spot. Fig. 8 presents these data. The size of the bright central region of the cyclone where the storm originated (Supplementary Text T1) is very similar to the size of the methane bright storm on 31 May 2020. Thus, the entire cyclone was affected by the strong outbreak.

The evolution of the area of the storm A, can be used to calculate the divergence of the flows associated to the storm activity, $Div\ V$.

$$Div\ V = \frac{1}{A}\frac{dA}{dt} \tag{2}$$

This results in maximum divergences of $\sim 8.0 \times 10^{-6}$ s^{-1}. This term can be related to the intensity of updrafts in convection. Following Hunt et al. (1982):

$$w \geq H\ Div\ V \tag{3}$$

where t is time, H is a scale height, ~20 km at 500 mb, and w is the minimum vertical speed required to explain the divergent flux. These values result in global estimates of $w \geq 0.15$ ms^{-1}, which is comparable to intense convective storms of different sizes in the giant planets (Hunt et al., 1982, Sánchez-Lavega et al., 2011). However, true vertical velocities in updrafts are expected to be significantly larger and can scale up to two orders of magnitude higher if convection is limited to small updrafts inside the main convective storm (Hueso et al., 2002).

A polynomial fit to the longitudinal and latitudinal size of the storm evolution results in a smooth divergence of the cloud field with an activity in two peaks (Fig. 8a). The first peak (shadowed area in Fig. 8) is calculated assuming that the storm started its eruption one Jupiter rotation before its discovery with an initial size of the cyclone equivalent to its size in April. If the storm erupted only a few hours before its discovery, its initial divergence could be larger. The second peak reflects a more slowly expansion well constrained by HST and Junocam observations. The double peaks in divergence have some similarities with the series of convective pulses that developed in 2018 in the storms in the STB Ghost (Iñurrigarro et al., 2020). This double peak also agrees with the observed evolution in methane-band images. This is: (1) An explosive onset at the time of the first amateur observations. (2) A fast decrease of brightness and contrast in amateur methane-band images. (3) A second outburst of convection shortly before HST observations, supported by the characteristics of the HST images with the visibility of bright cores inside the storm and the bright methane band and UV images. (4) Lower activity at the time of Junocam observations, when the methane band image shows the storm as bright compared with its environment, but much less bright than many other methane-band features observed by Junocam during the mission.

Taken together, the global evolution observed on ground-based images in the methane band, the wind measurements derived from Junocam images, and the size expansion shown in Fig. 8, suggest the storm had stopped active convection, or was close to stopping its strongest vertical motions when Junocam observed it.

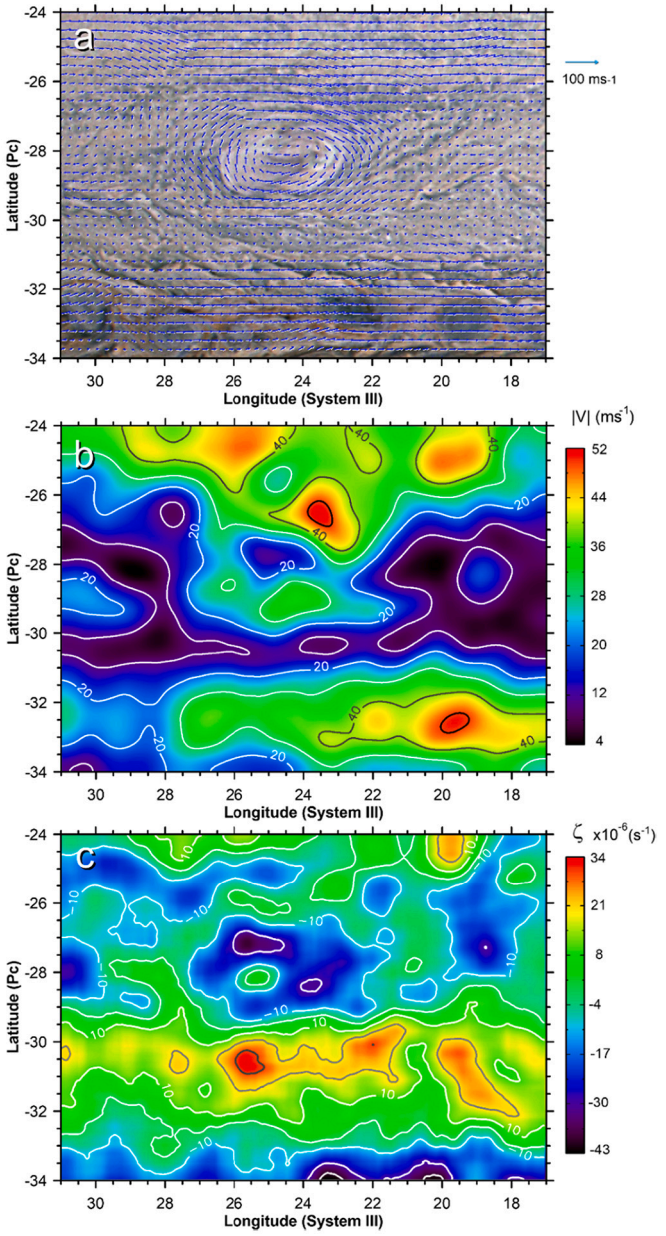

Fig. 7. Wind field retrieved from Junocam images. See method details and caveats described in the text. (a) Morphology of the cyclone with wind vectors. (b) Wind speed. (c) Vertical component of the relative vorticity associated to the motions. All wind fields in this figure have been smoothed to a spatial resolution of one degree and structures with smaller scales are not significant.

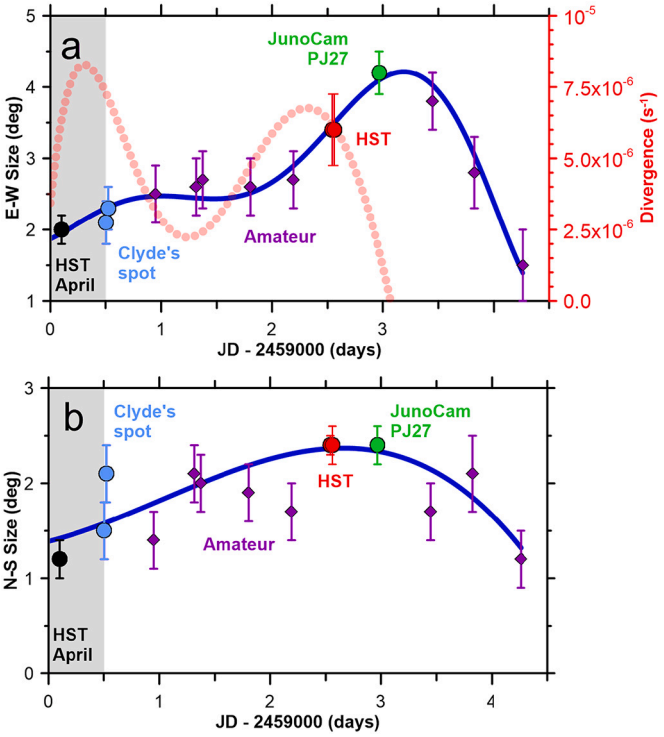

Fig. 8. Size evolution of Clyde's Spot in its East-West (a) and North-South extension (b). The black dot on the left part of the panels represents the size measurement on images acquired on April 11, 2020, and the grey area highlights that the growth rate in this period is more uncertain and could be significantly higher. The red dotted-curve on (a) shows the observed divergence from the size expansion (see text). (For interpretation of the references to colour in this figure legend, the reader is referred to the web version of this article.)

4. Temporal evolution of Clyde's Spot and DS6 in 2020

4.1. Transformation of Clyde's Spot into a dark feature

After the storm's outbreak, the bright clouds evolved in a time-scale of days to form a dark feature of a similar size to Clyde's Spot. This transformation possibly represents a fast clearing of the lower clouds associated with strong precipitation, and slow clearing of the upper clouds left by convection. Hints of these dark clearings are already observable on HST images in red wavelengths on June 2, 2020 (Fig. 5), with the cyclone darker in red wavelengths than its environment, but with a bright coverage of upper clouds visible in blue and UV wavelengths. Junocam images obtained 10 h later show the cyclone bright in broad filters and decaying in brightness in the methane band. Ground-based amateur images showed a highly contrasted dark feature that was known in the amateur community as Dark Spot 7 (DS7), or Clyde's Spot Remnant. Some examples of its complex evolution are shown in Fig. 9.

Morphological changes in Clyde's Spot/DS7 were accompanied by small-scale latitudinal oscillations and the production of small features that seem to have been emitted from it, or torn from it by the local winds. This kind of behavior has been previously observed in turbulent segments of the STB and FFRs in other latitudes (Li et al., 2004; Rogers et al., 2013; Rogers and Adamoli, 2015). The amateur data is good enough to track some of these very small features and the analysis of their motions is displayed in Supplementary Fig. S4. Most of the features that were apparently emitted from DS7 followed drift rates consistent with the zonal wind profile, and only a bright patch of material seemed to have been retained by the dark spot moving differently to the environment winds over a few days. The drift rate of DS7 was not linear, and it had some sharp changes in those instances when DS7 emitted some of these features. However, its average motion, as well as that of DS6, matched the zonal wind profile (Supplementary Fig. S4).

Further details of the morphology of DS7 and the DS6 vortex can be seen in HST images obtained in July, August and September 2020. Supplementary Fig. S5 shows examples of the July and August HST images. Fig. 10 shows the September HST images. In all these HST images DS7 is darker than its environment in UV, and both DS6 and DS7 are darker than their environments in the strong methane absorption band in 890-nm. However, small-scale bright filaments in DS7 are visible in all these HST images and all wavelengths in the periphery of the cyclone. These are comparable to bright filaments in methane-band images of the 2018 STB storm described in Iñurrigarro et al. (2020), and may represent sustained low intensity convection in the outer edges of the cyclone. DS7 also shows a turbulent wake down-wind on its west side that extends down to DS6.

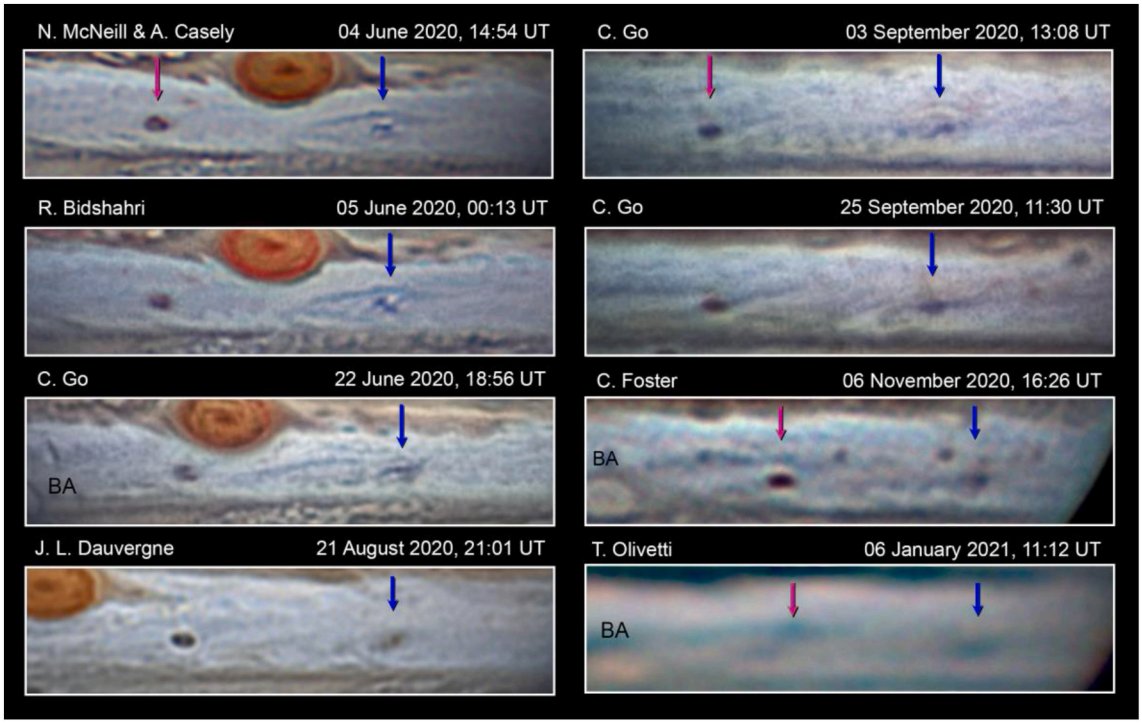

Fig. 9. Observations of the evolution of Clyde's Spot after the dissipation of the convective storm and its transformation into a dark remnant (DS7), indicated in all panels with a blue arrow. The position of DS6 is indicated with a purple arrow, and Oval BA is indicated when present. The image acquired on 6 January shows both cyclones close to Jupiter's solar conjunction. (For interpretation of the references to colour in this figure legend, the reader is referred to the web version of this article.)

The HST observations captured in September 2020 show DS7 close to the central meridian of the planet in two different views separated by a full planetary rotation. We examined these images identifying common features highlighted in Fig. 10b and c. For each individual feature, we built an ellipse with a fixed eccentricity taken from the overall shape of the vortex and we calculated the velocity of the cloud feature by considering the full arc travelled by the cloud feature between both images. The analysis of about 10 tracers shows a rotation curve that confirms the cyclonic nature of the vortex with an outermost velocity of 50–60 ms^{-1} at a distance of ~3000 km of the cyclone's center. This velocity is larger than the overall velocities measured from Junocam images of the storm and we cannot resolve if the dark remnant intensified its circulation, or if the analysis of the Junocam images did not achieve the real peak velocities of the structure. A possible explanation of these higher velocities that reconciles Junocam and HST measurements is that HST images may reflect the motions of deeper clouds closer to the vortex midplane, while Junocam may have observed the motions of higher altitude clouds just after the convective eruption. For each velocity measurement, a mean vorticity can be obtained using the circulation theorem and considering constant velocity across the ellipse fit for each tracer. The statistical analysis of the ensemble of measurements results in an overall relative vorticity of $-(3.6 \pm 0.7)x10^{-5}\ s^{-1}$, similar to the peak vorticities on the Junocam images in Fig. 6, but here representative of the overall vorticity of the structure.

We also note that the storm's remnant in September 2020 is significantly larger than the original Clyde's Spot in May 2020, and equivalent to the storm observed by Junocam in early June (Fig. 8).

After the dissipation of the initial Clyde's Spot convective outbreak, both DS6 and DS7 were low albedo features in red wavelengths and in methane band images. We looked for these features in 5.1 μm images obtained regularly at the IRTF and found that both cyclones were bright features with low cloud opacity during 2020 (Fig. 11). This indicates major changes in both cyclones since 2019, when the precursor cyclones to DS6 and DS7 were barely observable at 5.1 μm (Supplementary Fig. S3). For DS7 these changes at 5.1 μm can be associated with precipitation during convection. However, no signature of moist convection was found in DS6 in our extensive survey of 2019 and 2020 images.

5. Longer-term evolution of Clyde's Spot and DS6 in 2021

After solar conjunction new observations of Jupiter showed important changes in both DS6 and DS7. Fig. 12 shows Junocam observations of the STB obtained on April 15, 2021 (PJ33). DS7 had transformed from the dark cyclone surrounded by turbulent bright clouds observed during the second half of 2020 into a complex larger structure reminiscent of a FFR. FFRs tend to form in regions of high meridional wind shear and the morphology of DS7 follows a turbulent pattern consistent with the structure of the zonal winds (Fig. 12b). The change of DS7 into a complex FFR might have been triggered by its slow latitudinal expansion and its interaction with the zonal winds. The expanded size of this FFR compared with Clyde's Spot, or its dark remnant DS7, suggests continuous or episodic convective activity much later than the strong convection episode that made Clyde's Spot.

Unlike DS7, DS6 was not immediately evident after solar conjunction and seemed to have disappeared. However, Junocam images obtained on April 2021 showed a new oval with an orange inner region surrounded by a white collar present just north-east of Oval BA in the cyclonic shear of the zonal winds (Fig. 12b). Methane band images of this cyclone show it as a dark feature with low clouds (Fig. 12c). We identify this new cyclonic oval as the transformed DS6 from its long-term tracking and the absence of additional candidates to form this cyclone. For convenience, we will name this feature White Spot 6 (WS6) to recall its origin and bright aspect.

Junocam observed this area again in its next perijove (PJ34) on June 8, 2021. We obtained images with the IRTF, Gemini North, and the PlanetCam instrument on June 7 under good seeing conditions. Fig. 13 shows a Junocam observation of the region and a combination of IRTF and Gemini North images in 4.7–5.1 μm. Supplementary Fig. S6 shows

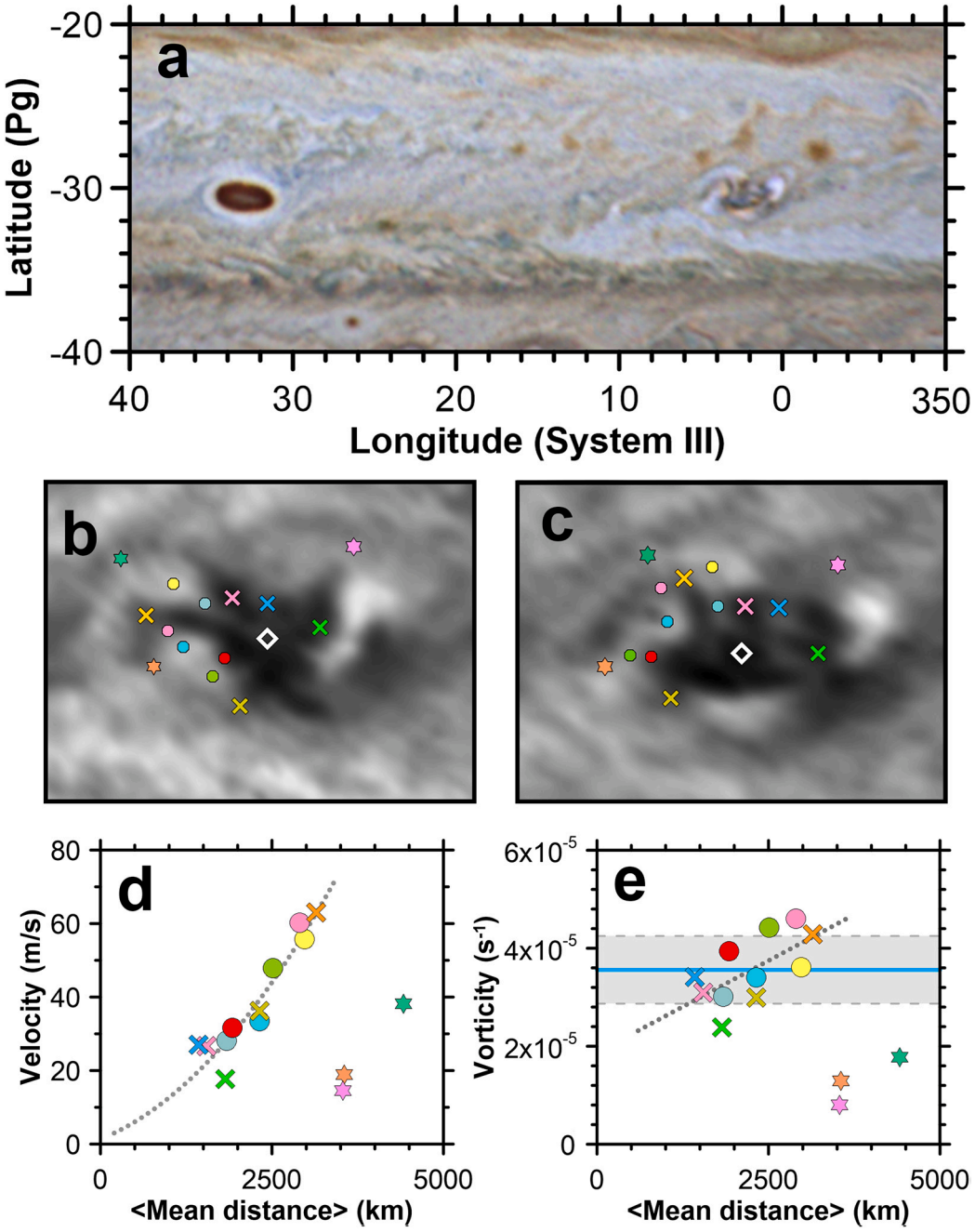

Fig. 10. HST observations of DS7 from 20 September 2020. (a) Map showing DS6 (left) and DS7 (right). (b) and (c) Magnified views of DS7 obtained with the F631N filter with a time difference of a planetary rotation. Symbols identify different features visible in both images. A white rhombus shows the center of the oval. (d) Velocities of the different features identified in (b) and (c). (e) Vorticities of individual features. The three features identified with stars in b-e do not follow the same motions pattern and constitute wrong identifications or features outside the vortex.

PlanetCam images from 380 nm to 1.7 μm. The FFR had continued to expand and WS6 was further away from Oval BA than in the previous perijove with small changes in its overall aspect, but keeping its outer ring of brighter material. Thermal infrared images (Fig. 13b) show DS7 as a bright feature with an inner structure that roughly matches the dark albedo patches observed in the visible (Fig. 13a). The Gemini image shows significant structure in the FFR, with bright and dark patches that can correspond to bright cloud clearings (dark in visible images) and dense clouds (bright in visible) that are much smaller than the cloud-free regions, and where new clouds and limited vertical convection could still be occurring. The reddish cyclone WS6 was not visible at 5.1 μm, contrasting with its high brightness at this wavelength in October 2020 (Fig.11). A pair of anticyclones, dark in the visible and bright in 5.1 μm are also seen in these images southeast of WS6.

Further observations of the area were obtained by Junocam in the next perijove (PJ35) on July 21, 2021 and covered Oval BA and WS6 (Fig. 14a). The FFR remnant of Clyde's Spot was best observed by PlanetCam (Fig. 14b and Supplementary Fig. S7) and IRTF (Fig. 14c) images. PlanetCam images in the visible showed an expanding pattern of bright and dark features that we interpret as the transition from the FFR observed in PJ34 into a turbulent segment of the STB. This turbulent area is a bright region in IRTF images at 5.1 μm. Additional bright features in 5.1 μm images observed at PJ35 are highlighted with green and purple arrows in Fig. 14. The largest of these features (green arrow in Fig. 14) is possibly the merger of the two smaller anticyclones observed on PJ34.

Junocam offered a clear view of Oval BA and its interaction with the pale cyclone WS6. On July 21, 2021 both features were near their closest approach, and their separation was equivalent to the Rossby deformation radius, L_d, which is a measure of the distance at which atmospheric systems can sense each other and interact. L_d is $NH/|f|$, where N is the Brunt-Väisälä frequency, $\sim 10^{-2}$ s^{-1} at cloud level (Lindal et al., 1981),

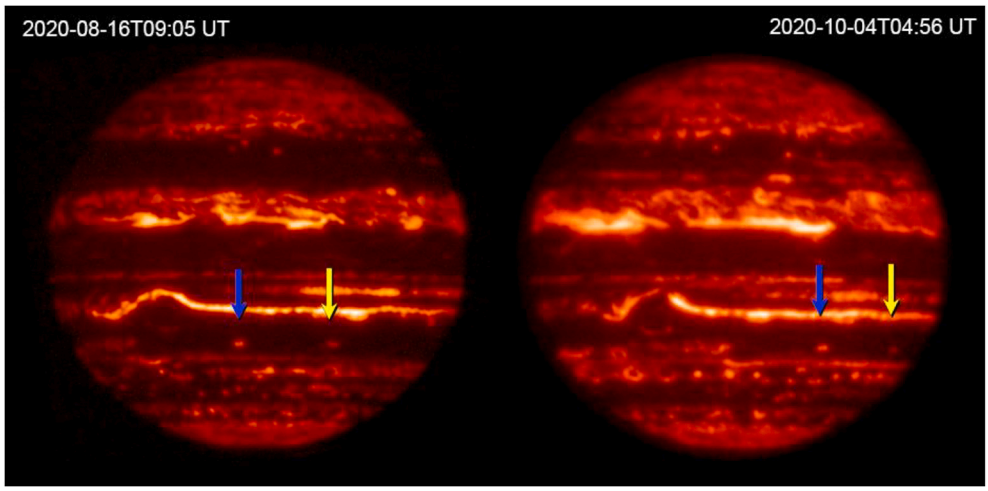

Fig. 11. IRTF 5.1-μm images of DS6 (blue arrow) and DS7 (yellow arrow) in 2020. (For interpretation of the references to colour in this figure legend, the reader is referred to the web version of this article.)

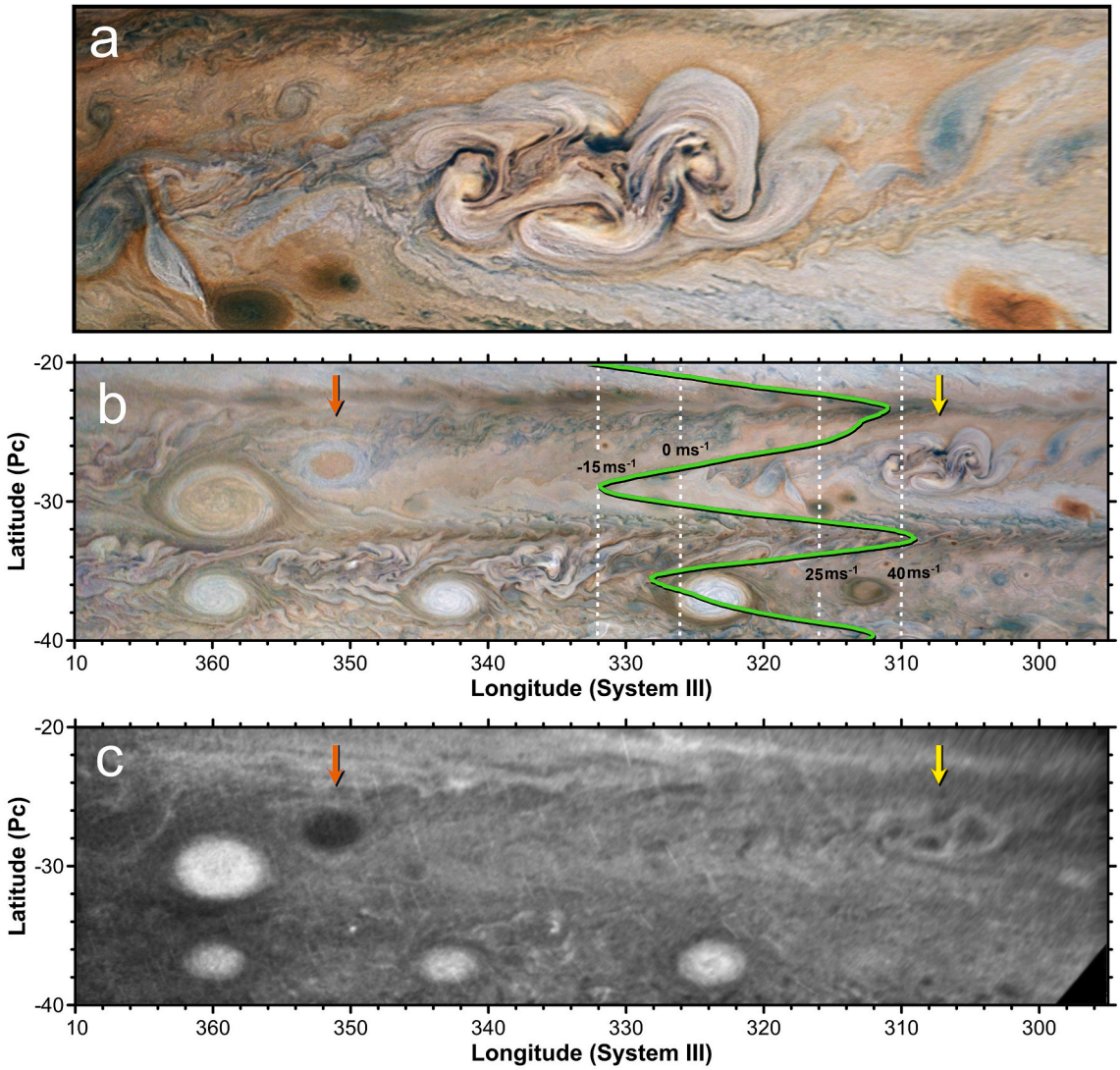

Fig. 12. Junocam observations from PJ33 on April 15, 2021. (a) Detailed map of the remnant of Clyde's Spot (DS7) transformed into a highly turbulent region. (b) Map of the STB from Oval BA to the remnant of Clyde's Spot. The zonal wind profile is overplotted in green with zonal winds grid lines in white. (c) Same as panel b, but in methane band. Orange arrows show the vortex candidate to be the long-term remnant of DS6/WS6, which was bright white in amateur images. (For interpretation of the references to colour in this figure legend, the reader is referred to the web version of this article.)

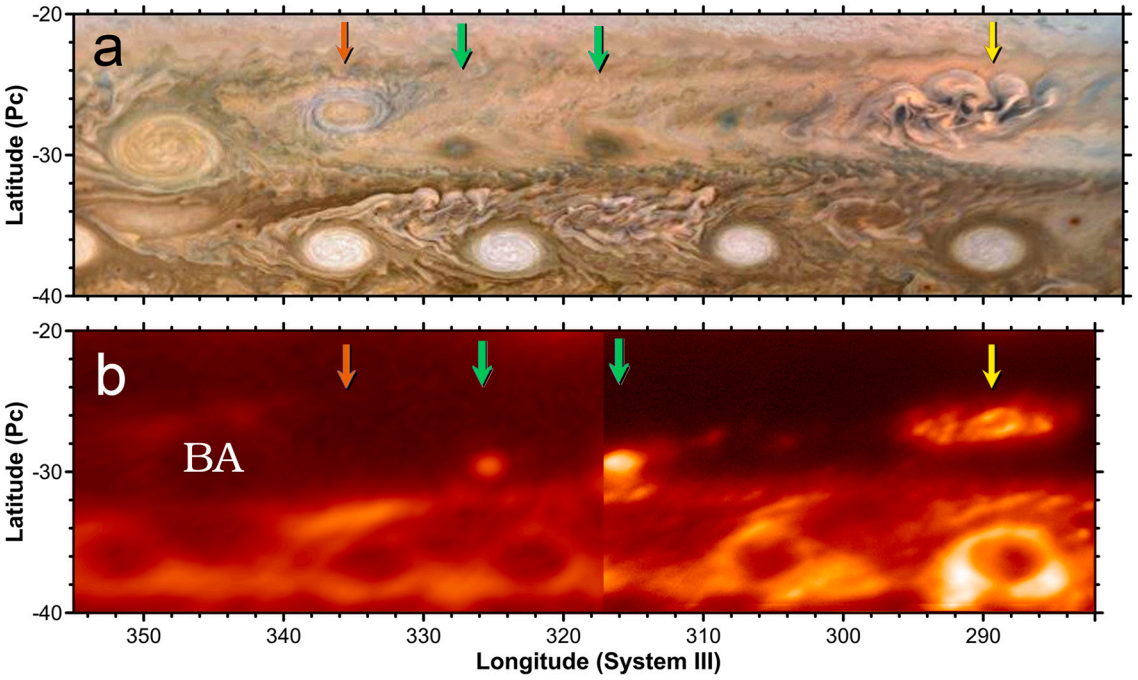

Fig. 13. Multi-wavelength observations obtained on June 7–8, 2021 covering PJ34. (a) Junocam map in visible wavelengths. (b) Thermal infrared map based on IRTF at 5.1 μm images (left-side) and Gemini North 4.7 μm images (right-side). Orange and yellow arrows show WS6 and Clyde's Spot Remnant. Green arrows show new ovals, possibly anticyclones by their latitudinal location. (For interpretation of the references to colour in this figure legend, the reader is referred to the web version of this article.)

H is pressure scale height, ~22 km at cloud level, and $f = 2\Omega sin(\phi) = 1.8 \times 10^{-4}$ s^{-1} is the Coriolis parameter with angular rotation $\Omega = 1.76 \times 10^{-4}$ s^{-1} at latitude ϕ). This results in $L_d \approx 1200$ km or 1.2°, which is comparable to the distance between the outer rings of Oval BA and WS6. Since both features have opposite vorticity, WS6 started to separate from Oval BA in the days after these images were acquired.

Multi-wavelength PlanetCam observations of the STB are shown in Supplementary Fig. S7. Strong contrasts in UV and methane bands of the FFR feature are suggestive of active formation of new clouds in this evolved phase of Clyde's Spot. The pale WS6 cyclone is bright in UV and dark in methane bands, similarly to the cyclone where Clyde's Spot developed. At this stage, ground-based observations in the visible cannot precisely determine the zonal extent of the FFR, which continued to expand forming an elongated turbulent segment of the STB. HST obtained on 4 Sept. 2021 the best view of the complex evolution of Clyde's Spot during this phase (Fig. 1f).

The global set of observations here described and the multiple changes in the visual aspect of these features can be placed in context showing the temporal evolution of their positions. Fig. 15 shows the long-term tracking of Clyde's Spot and DS6/WS6 from their precursor vortices in 2019 to their latest positions in December 2021. Data for 2019 are discussed in Supplementary Text T1. Both Clyde's Spot precursor and DS6 were the outcome of vortex mergers in 2019. The Clyde's Spot precursor passed very close to the GRS a few days before its convective outburst in May 2020. DS6 also crossed south of the GRS about a month later with no changes in its aspect. However, DS6 transformed radically after solar conjunction in December 2020, becoming orange-white (WS6) and approaching very close to Oval BA.

Fig. 16 shows an enlarged version of the tracking of DS6/WS6 and Clyde's Spot remnant DS7 from June 2020 to December 2021. The tracking in longitude of both features are shown after subtracting linear fits to their longitudinal drifts in 2020 and show that both features substantially changed their drift rate in longitude over solar conjunction. DS7 changed its zonal drift from (−0.226 ± 0.002)°/day before conjunction to (0.296 ± 0.007)°/day after conjunction, possibly following a very small latitudinal drift northwards, and accommodating its drift rate to the zonal winds. DS6 changed its drift rate from (−0.233 ± 0.003)°/day before conjunction, to a more complex behavior after conjunction, when the feature appeared as a white cyclone (WS6). DS6 approached Oval BA and experienced a close approach around April 2021, when its morphology was already a white/orange feature (WS6). It later oscillated in its mean distance to Oval BA with a drift rate that varied from −0.18°/day to −0.41°/day with a mean value of −0.33°/day. This is close to Oval BA's drift rate after conjunction of (−0.296 ± 0.005)°/day. Changes in DS6/WS6 drift rate and its distance to Oval BA from April to August 2021 occurred without visible morphological changes accompanying these variations, they were not accompanied by visible changes in latitude, and may reflect the dynamic interaction between the anticyclonic Oval BA and the cyclonic DS6/WS6. However, in August 2021, the latitude of DS6/WS6 seemed to drift northwards ~0.5° (Fig. 16d) and started to separate from Oval BA.

Finally, Supplementary Fig. S8 shows measurements of the expansion of Clyde's Spot into a FFR and a turbulent segment of the STB. These measurements use only HST and Junocam images, where the limits of these features can be safely established from the images. The size of the turbulent segment of the STB in which Clyde's Spot had transformed in September 2021 was 15.5° in longitude and 5.7° in latitude (or ~ 115 × 10^6 km^2). This represents an area 35–40 times larger than the precursor vortex in April 2020, and 8.5–9.0 times larger than the size of Clyde's Spot as observed by Junocam on June 2020. It also represents a net expansion in area of ~230,000 km^2 day^{-1} sustained over 450 days after the explosive outbreak. However, probably most of the growth took place throughout 2021. For comparison, the explosive outbreak created fresh clouds at a much faster rate of 3,400,000 km^2 day^{-1} over only 3 days.

6. A new outbreak in Jupiter's STB

A new convective outbreak in the STB occurred on August 7, 2021. The convective activity started in a cyclone with a very similar morphology to the cyclone where Clyde's Spot developed. The storm started a few days after this new cyclone crossed south of the GRS. The

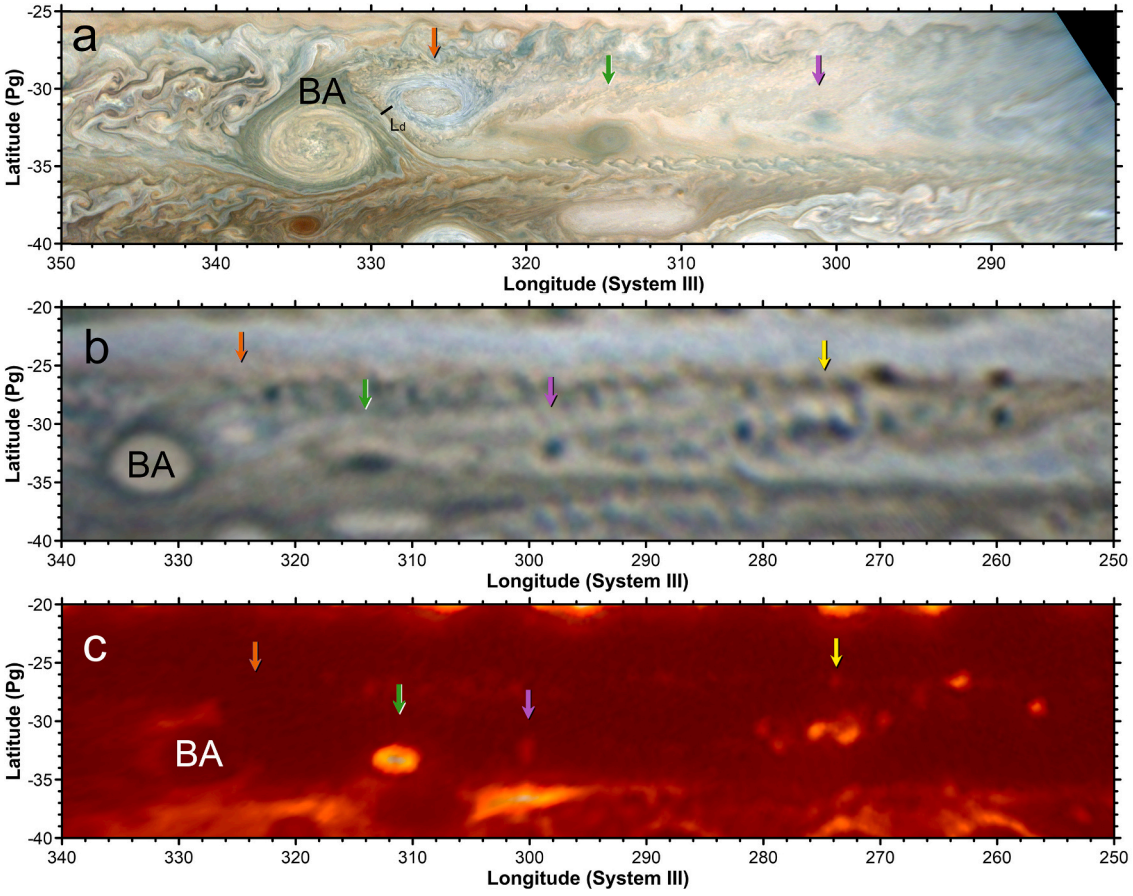

Fig. 14. Maps of the STB around Juno's PJ35. (a) Junocam (July 21, 2021). (b) PlanetCam image (July 20, 2021). (c) IRTF images at 5.1 μm (July 22, 2021). Yellow arrows identify DS7 on panels (b-c), orange arrows WS6 (the transformed DS6), green and magenta arrows indicate bright features at 5.1 μm and dark in visible wavelengths. The Rossby deformation radius, L_d, is marked on panel (a) and matches the distance between the outer structure of both Oval BA and WS6. (For interpretation of the references to colour in this figure legend, the reader is referred to the web version of this article.)

cyclone had become brighter in visible wavelengths in the previous days, but convection was not visible in methane band images until 7 August and quickly diminished in activity in a very similar time-scale to Clyde's Spot. Supplementary Fig. S9 shows early views of the storm's precursor, which was the possible result of mergers of different cyclones visible in the STB over 2020. Fig. 17 shows a summary of the early observations of this convective eruption. Fig. 2 shows later high-resolution views of the transformation of the storm, first into a turbulent feature similar to the early evolution of Clyde's Spot, and later into a closed dark cyclone.

The key features of this storm and its later evolution were:

- Sudden emergence of the outbreak in methane images of a small cyclone (Fig. 17a, b) with a fast decrease of the visibility in methane-band images (Fig. 17c).
- Formation of a double-sided bright cloud in visible wavelengths (Fig. 17e and f) 2 days after the outbreak, similarly to the observations of Clyde's Spot obtained by Junocam 2.5 days after the initial outbreak.
- Transformation of the bright clouds in a complex system with dark features and a turbulent pattern in a time-scale of 7–10 days (Fig. 17g, h, i). The new dark feature, seemed smaller than the one associated with Clyde's Spot remnant, but expanded into a turbulent dark region in a time-scale of about 3 months (Fig. 2c).
- Transformation into a close dark cyclone similar to views of DS6 over 2020. This transformation was not observed directly, as it occurred with Jupiter approaching solar conjunction, and the only clear view of the cyclones was the outcome of the changes in the images obtained by Juno on January 2022 (Fig. 2d).

We analyzed the original unprocessed observations of this storm acquired the day of its onset by C. Go with a telescope similar to the one used by C. Foster. The unprocessed photometric methane-band image showed the storm with an increased brightness of 13% over its surroundings. This larger contrast when compared with Clyde's Spot is explained by the narrower methane-band filter used by this observer. An evaluation of the storm cloud top altitude following the RLM as for Clyde's Spot results in a similar estimation of cloud tops about 0.25–0.30 scale heights above their environment (i.e. 4–5 km) and confirms a similar level of convective activity at the outbreak.

Fig. 18 shows the tracking of the cyclone where the storm developed and the later drift of the convective system. The system changed its drift rate continuously over 2020–2021 but these changes were accompanied by small changes in latitude (Fig. 18b), and the different drift rates of this meteorological system were always in agreement with the zonal winds and can be explained by a small northward migration from −31.0 ± 0.5° in March–June 2021 to −30.3 ± 0.5° in August-2021-January 2022.

A comparison of latitudes, drift rates and zonal winds of Clyde's Spot, DS6 and the 2021 STB storm and their precursor systems is shown in Supplementary Fig. S10. In general, these cyclonic systems (Clyde's Spot over its different phases, DS6 also with its different morphologies and colour, and the 2021 STB storm) present small changes in latitudes that explain their different drift rates in longitude. The origin of these latitudinal migrations are probably related with interactions with the

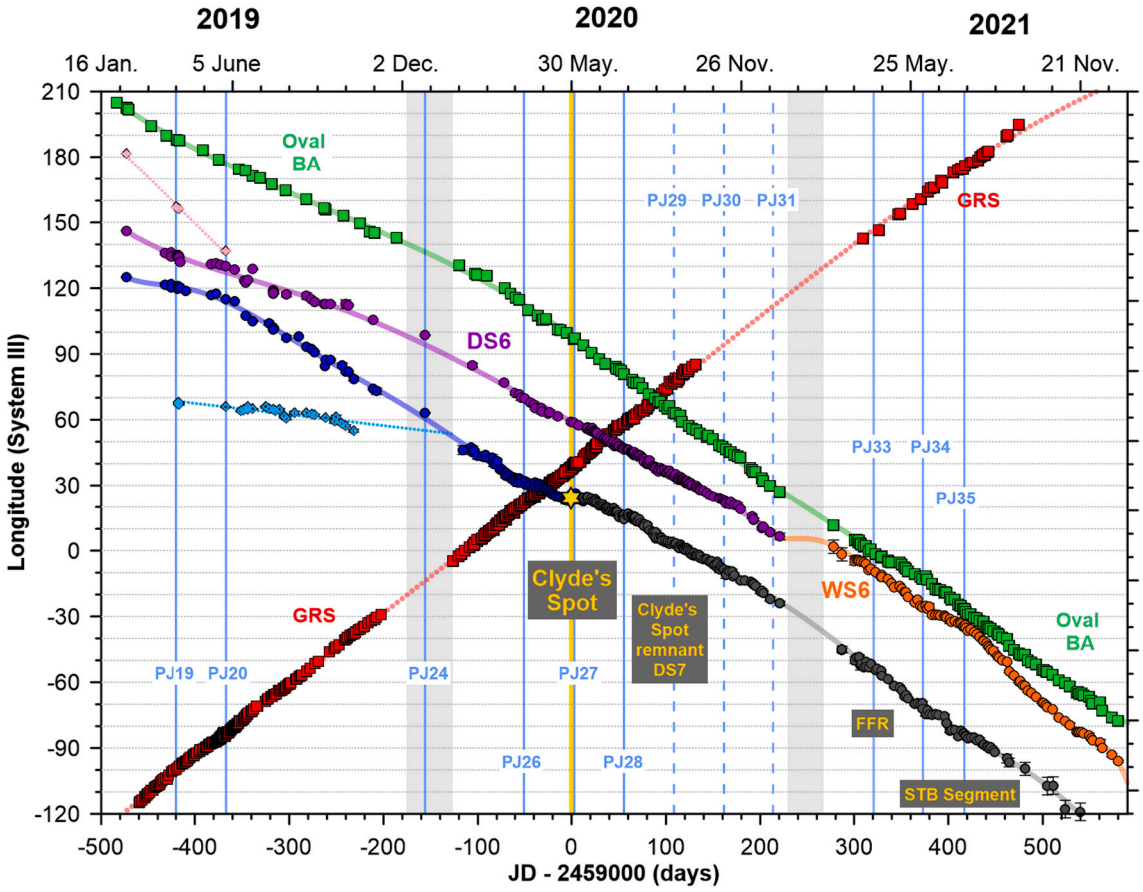

Fig. 15. Tracking of Clyde's Spot, DS6 and related features over 2019–2021. Vertical lines indicate Juno's perijoves with data used here. Grey regions indicate Jupiter's solar conjunction. The positions of the GRS are based in data presented by Sánchez-Lavega et al. (2021).

fine-scale structure of the zonal jets, instead of the beta-drift mechanism, since some of these cyclones migrated equatorward and some others poleward. We also note that the STB jet is interrupted by the presence of the large Oval BA (Fig. S2), and this large anticyclone had a variable drift rate over 2019–2021 (Fig. 15).

Constraining the size evolution of this storm and its evolution is more difficult than on Clyde's Spot. Supplementary Fig. S8 shows the size evolution of Clyde's Spot and the 2021 STB storm over their different phases and show they were both comparable over the first 150 days of each event.

All in all, this storm was very similar to Clyde's Spot, with minor differences in its early stages, initial size and drift rate. However, its later evolution was remarkably different with the formation of a dark cyclone similar to DS6. Both, Clyde's Spot and this second storm migrated northwards in a comparable manner after the storm's onset but the 2021 STB storm showed signatures of lower convective activity. However, because the observational data for this storm is not of the same quality as for Clyde's Spot, we defer a more extensive analysis of the observations of this feature.

7. Comparison with similar storms in closed cyclones

The complex phenomenology of Clyde's Spot and the 2021 STB convective storms can be compared with the evolution of previous storms formed in closed cyclones. In 2018 a series of convective storms appeared in a time-scale of a few days in the elongated cyclone known as the "STB Ghost". The storms and the later complex evolution of the cyclone are described by Iñurrigarro et al. (2020). In the 2018 STB Ghost, 2–3 convective outbursts developed over a few days and produced significantly more bright clouds than in the 2020 event analyzed here. Those clouds followed partly the circulation of the pre-existing cyclone forming elongated clouds (Fig. 18 in Iñurrigarro et al., 2020) very different from the double-sided storm observed by Junocam in June 2020 (Fig. 6c), or the double-sided storm observed by amateurs in August 2021 (Fig. 17f). As a consequence of the convective storms, the 2018 STB Ghost developed a highly turbulent structure with the formation of very dark features and bright filaments that quickly mixed with the elongated STB Ghost, disturbing its morphology over months. The STB Ghost approached the west side of Oval BA, merging with a previously existing cyclonic cell and leaving a long turbulent segment in the STB still present in Jupiter with a remarkable evolution of morphology in 2020 (Supplementary Fig. S9) and 2021 (Supplementary Fig. S7).

In the 2018 storm in the STB Ghost, Clyde's Spot in May 2020 and the August 2021 storm, the sudden convective outbreak initiated a persisting pattern of turbulence in each of the cyclones that later expanded fully transforming these cloud systems. In the 2018 STB Ghost and Clyde's Spot remnant, HST images in the methane band show bright filaments observed months after the convective outbreaks that could be indicative of sustained moist convection. This sustained moist convection might be needed to explain the increase in size of Clyde's Spot Remnant in its FFR phase, and the strong contrasts in visible and infrared images during PJ34 in June 2021 (Fig. 13).

A remarkable aspect of Clyde's Spot is how it formed a double-lobed cyclone days after the convective eruption, and how it evolved into an FFR-like structure a year after. Voyager 2 observed a similar convective outbreak lasting about 30 h in a pre-existing cyclonic oval, but in the South South Temperate Belt (SSTB) at 38.8° S (Smith et al., 1979). In this case, the storm produced a two-sided lobe feature that quickly evolved to form an FFR in a timescale of a few days and achieved a stable

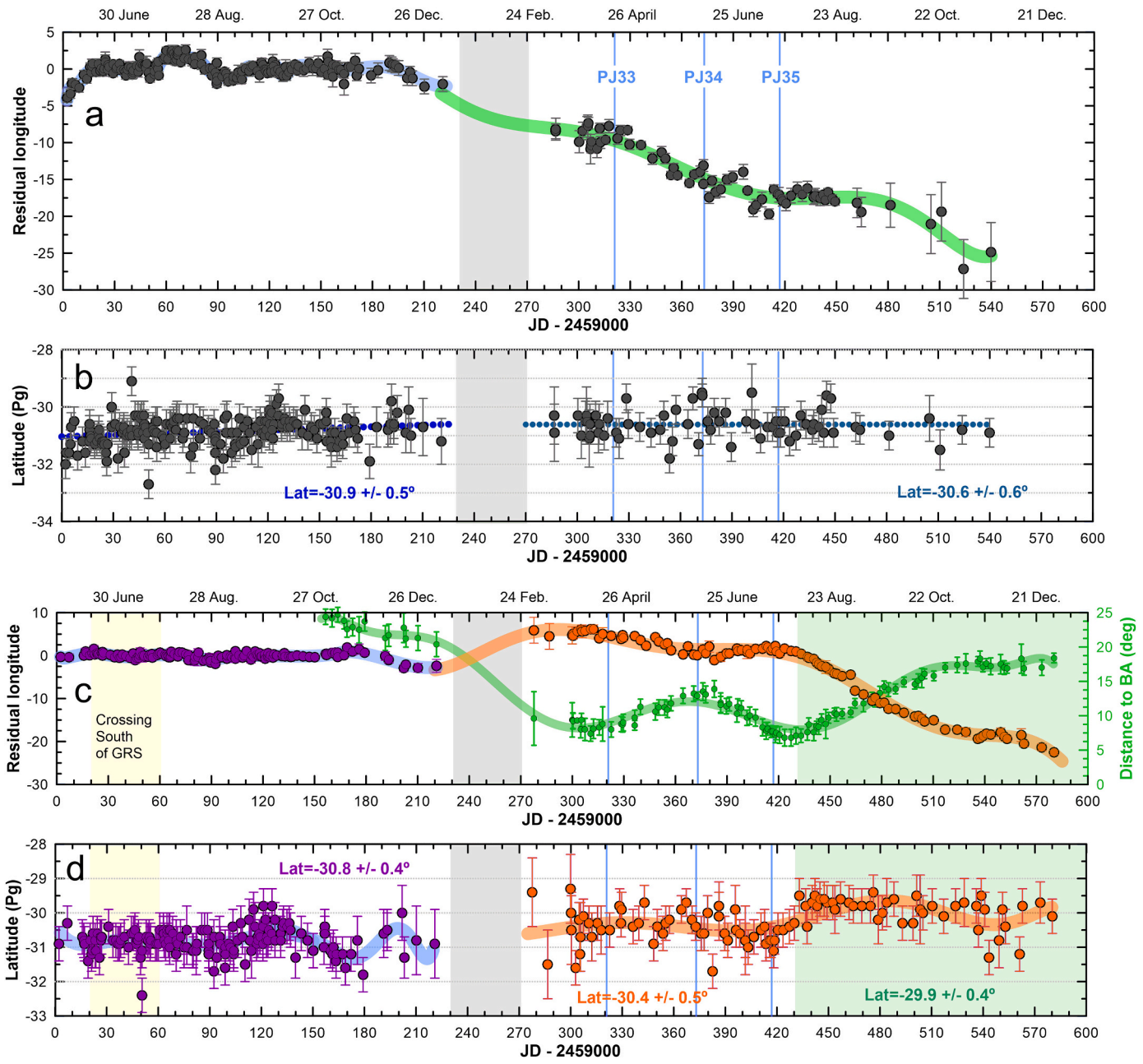

Fig. 16. Tracking of Clyde's Spot remnant (panels a and b) and DS6/WS6 (panels c and d). Panels a and c show residual longitudes after subtracting linear fits in 2020. Panels b and d show planetographic latitudes. Continuous lines show polynomial fits to the data. Dotted-lines in b shows linear fits to the data in each period. Panel c also shows the distance in degrees between the pale cyclone WS6 and the central meridian of Oval BA with small green circles and a polynomial fit to those data. Grey areas show solar conjunction, yellow areas the passing of DS7 south of the GRS, and the green area in panels c and d denote a distinct period of time during which WS6 changed its latitude and drift rate and finally separated from Oval BA. (For interpretation of the references to colour in this figure legend, the reader is referred to the web version of this article.)

structure in just a few weeks. Fig. 19 shows Voyager 2 observations of this storm and its transformation into a FFR. Just as in Clyde's Spot and the 2021 STB storm, this storm grew quickly, with a bright convective core with a size of about 1.5°x1.3°, and was active for a brief period. However, its activity resulted in permanent changes and intense turbulence in the region where it originated. Some tracers in the Voyager 2 image sequence suggest rotation of the turbulent filaments with velocities on the order of 35 ms^{-1}, thus, comparable to the wind motions we have obtained for Clyde's Spot.

8. Discussion

The convective cyclones in the STB studied here developed in closed cyclones, showed the simultaneous evolution of bright clouds and dark clearings after the outbreak, and had complex evolutionary tracks. One of them evolved expanding into a FFR and growing into a turbulent segment of the STB, and the other formed first a turbulent eddy that later evolved to form a stable dark cyclone. In this sense, we can wonder if the transformation of DS6 from a white cyclone in 2019 into a reddish cyclone at the start of 2020 could have been triggered by a convective event near solar conjunction in 2019.

Red cyclones like DS6, and FFRs like the result of the evolution of

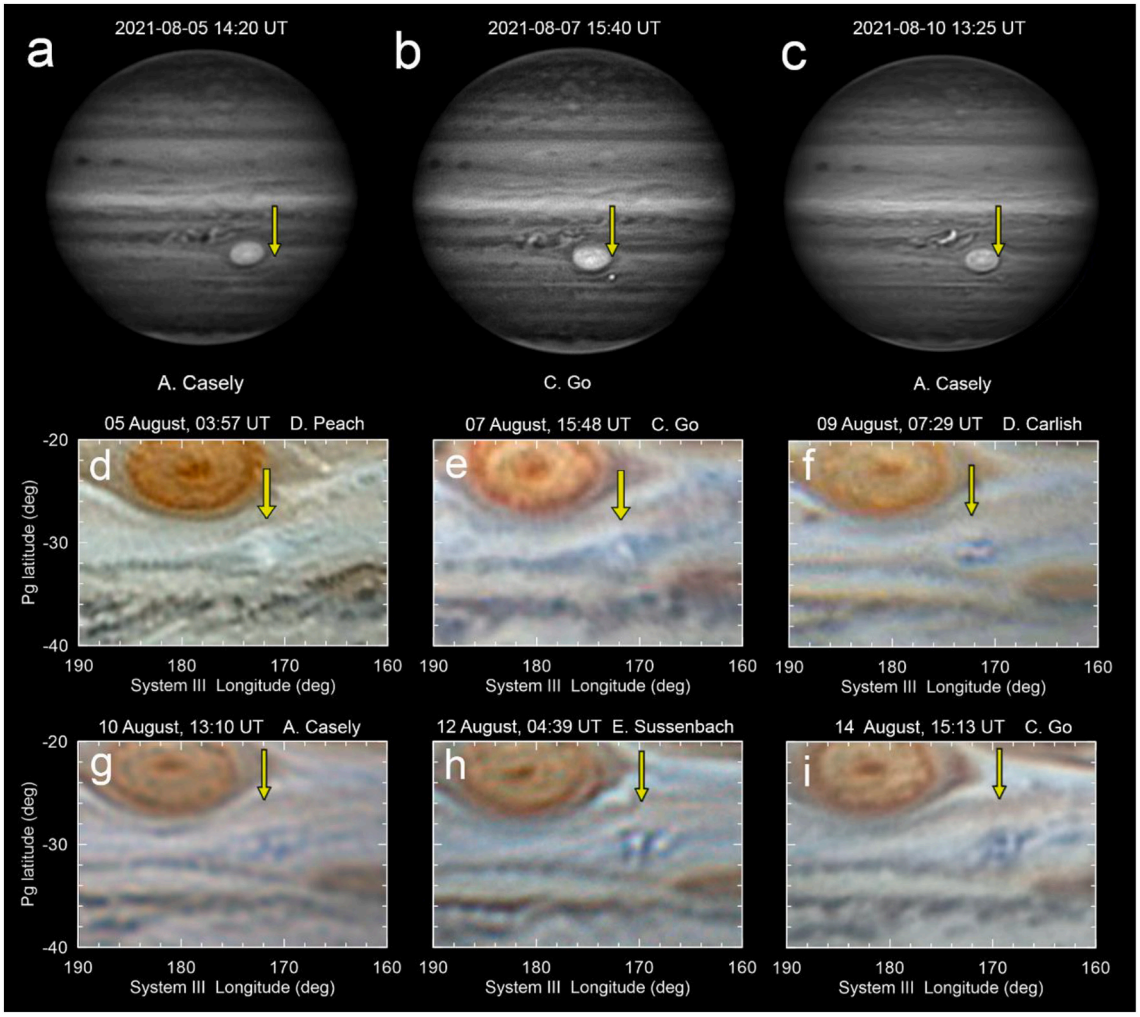

Fig. 17. Observations of a new outbreak in a cyclone in the STB in August 2021. (a) Methane band image 2 days before the outbreak. (b) Methane band image possibly close to the peak of the convective activity. Many other amateur observations obtained that day confirm the remarkable brightness of the feature. (c) Decay in brightness in methane band images. (d-i) Observations in visible wavelengths of the cyclone with no active convection (d), at the peak of activity (e), with a double-sided shape reminiscent of Clyde's Spot as observed by Junocam (f), and its later evolution into a complex dark feature (g-i).

Clyde's Spot are relatively uncommon in Jupiter's STB. Similar features were observed in 1994–1998 in HST images, when a dark oval seemed to form from a larger cyclonic cell constrained by the positions of the large anticyclones FA and BC with some moments of apparent increased brightness (Simon et al., 2015; Rogers, 2016). However, the time coverage of the observations of those features in 1994–1998 is not adequate for an in-deep analysis. Instead, here we have seen a complex evolution in which cyclones formed east of Oval BA in 2019 merged to form the precursors to DS6 and Clyde's Spot. DS6 experienced large changes on its own without observations of active convection, but those changes occurred close to solar conjunction. This cyclone transformed from a white cyclone in 2019 to a red dark cyclone in 2020, and then to a white feature. The later transformation occurred at the time of a strong interaction with Oval BA. Clyde's Spot formed inside a regular bright cyclone at the same latitude of DS6. This cyclone had low contrast in the visible but an elevated brightness in UV shared with cyclones at other latitudes that also develop convection (de Pater et al., 2019).

Wong et al. (2020) present a summary of recent HST and Gemini NIRI observations of Jupiter in the context of the Juno mission and discuss modern views of the relation between cyclones, convective storms and Juno observations of lightning and condensables. In particular, lightning flashes detected by Juno's Microwave Radiometer are located within cyclonic regions including FFRs, and HST observations in the continuum, and weak and strong methane absorption bands are used to infer the presence of deep clouds in these cyclones (Fig. 12 in Wong et al., 2020). The relations between moist convection and cyclones has also recently been discussed by Fletcher et al. (2017) and Thomson and McIntyre (2016), following arguments that vertically stable layers can be weakened in low-pressure cyclonic regions. Isentropes (surface of constant potential temperature) might rise in the deeper layers of cyclonic regions at cloud level favoring ascent of deep water that could initiate moist convection (Dowling and Gierasch, 1989).

The two storms in the STB studied in this paper (Clyde's Spot in 2020 and the 2021 STB storm) started in cyclones that were very similar. Both cyclones were the result of the merger of pre-existing smaller cyclones (Fig. S2 and Fig. 15 for Clyde's Spot and Fig. S9 for the 2021 STB storm), and in both cases convection started within 15 to 30 days after the storm passed the GRS central meridian.

It is unclear whether the result of a merger of two cyclones would result in a cyclone with a different vertical structure or distribution of deep condensables capable of developing convection. However, it is unlikely that vortex mergers trigger convection directly because the mergers occurred months before the onset of convection.

Fig. 20 explores the possible interaction between the GRS and the cyclones were storms developed in May 2020 and August 2021, as well as DS6. The three vortices had comparable latitudes within the measurement error at the time of their passage below the GRS. However, only the two vortices that later developed convective outbursts (Clyde's

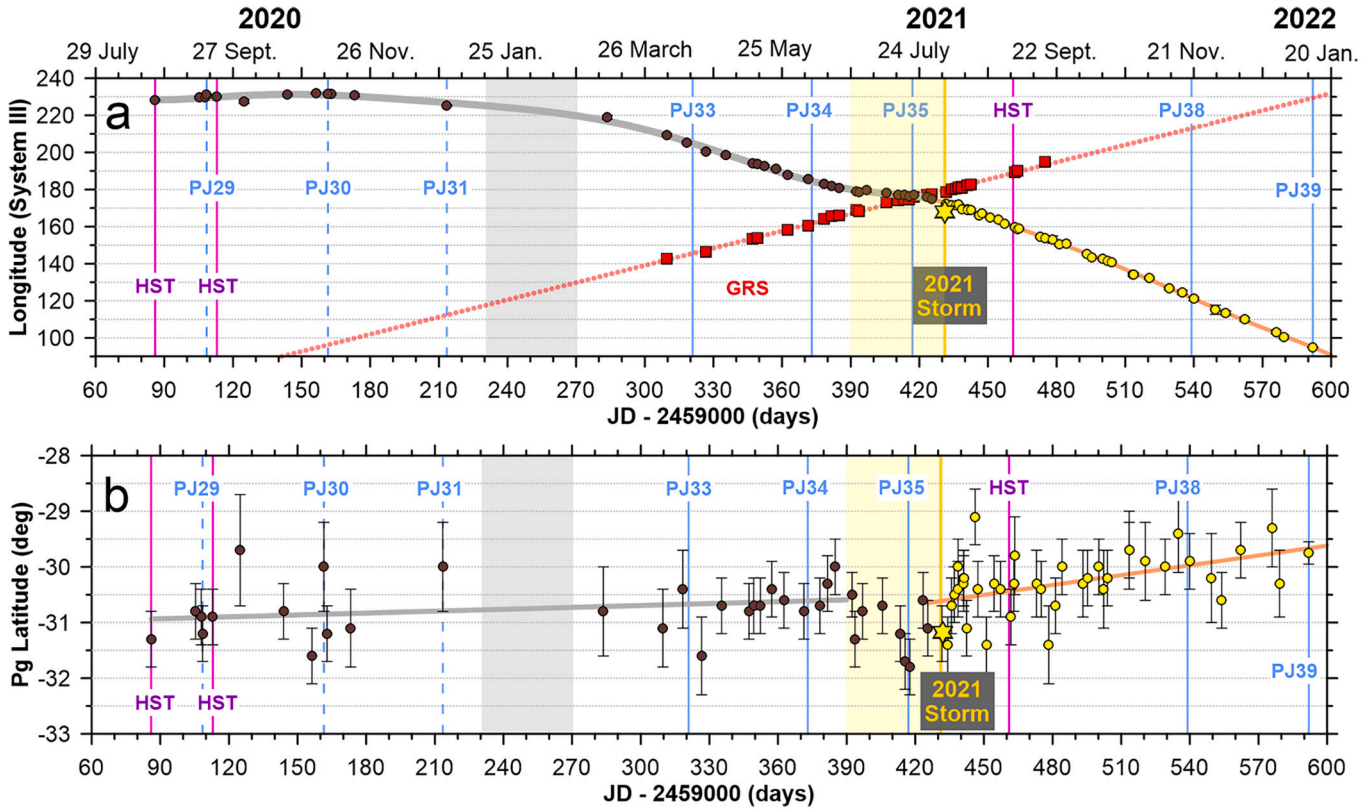

Fig. 18. Tracking of the 2021 STB storm. (a) Longitudinal tracking. (b) Latitudinal tracking. Blue vertical lines indicate Juno's perijoves. Magenta lines dates of HST observations. The grey region indicates Jupiter's solar conjunction. The yellow area shows the interaction of the storm's precursor with the GRS. The storm outbreak is shown with a star and a vertical yellow line. The cyclone where the storm started is shown with brown circles, the storm after its onset with yellow circles and the GRS is shown with red squares. Fits to the vortex latitudinal position before its interaction with the GRS and after the convective eruption are shown with grey and yellow lines respectively. (For interpretation of the references to colour in this figure legend, the reader is referred to the web version of this article.)

Spot and the 2021 STB storm) experienced a visible interaction with the GRS. Both cyclones changed their longitudinal drift rates, moved about 1° southward, and recovered their initial drift rate and latitude afterwards, just a few days before developing convective clouds. During the times these cyclones were displaced southwards both cyclones moved slightly more slowly than at their original latitudes and slightly faster than the zonal winds at their southernmost latitudes (Fig. 20g). The cyclone where Clyde's Spot developed interacted with the GRS more strongly than the precursor of the 2021 STB storm. DS6 did not show any signature of an interaction with the GRS in spite of sharing the same latitude as Clyde's Spot. This fact points to interactions between the GRS and the cyclones that would develop convection at deep levels below the upper observed clouds.

During the southwards excursion of these vortices we can hypothesize that they might have experienced compression effects caused by the drag with the external winds. This drag and compression might have helped the cyclones to deepen into the lower atmosphere by conservation of potential vorticity. Conservation of total vorticity implies that the southward migration of about 1° would have reduced the cyclonic vorticity of the cyclones by $\Delta\xi \approx 0.5 \times 10^{-5}\ s^{-1}$, which in turn, would have decreased their internal velocities by $\Delta v \approx (r/2)\Delta\xi \approx 5 - 10\ ms^{-1}$ (here uncertainties correspond to uncertainties in the size of the vortices). Unfortunately, details of this interaction are missing with only lower-resolution amateur images of the process available.

In any case, convection developed days after both cyclones recovered their initial latitude. In the case of Clyde's Spot, images of the vortex before the passage south of the GRS, and after this passage but before the onset of the storm, show no differences in the cyclone. Similar convective events in closed cyclones, like in the STB Ghost in 2018 or in the SSTB in 1979 do not require changes in latitude, or interactions with external cloud systems. Thus, it is unclear the role that the GRS could have had in triggering convection in Clyde's Spot and the 2021 STB storm.

One important result of the long-term evolution of Clyde's Spot is its slow but large expansion into a FFR and a turbulent segment of the STB. The net expansion rate of this cloud system, ~230,000 $km^2\ day^{-1}$, is ~6% of the expansion rate of Clyde's Spot during the 3 days of intense convective activity in May–June 2020. The net area divergence $1/A(dA/dt)$ of this slow expansion is equivalent to 1% of the values during the convective outburst. The coexistence of bright and dark features in HST methane band images, and the high and low opacity regions observed at 4.7–5.1 μm (Fig. 14c) suggest active convection extended over time. In ground-based methane-band images the FFR sector is darker than the STB, while it is slightly brighter in UV images. Together these observations reflect overall lower cloud tops than the STB. A possibility is that weak convection at the ammonia cloud layer drives the long-term expansion of Clyde's Spot, whose energetic outburst and high cloud tops point to convection driven by water condensation.

Both Clyde's Spot and the 2021 STB storm share many aspects with, but also differentiate themselves from convective outbursts in the STB Ghost in 2018 (Iñurrigarro et al., 2020) and in the SSTB in 1979 (Smith et al., 1979). Table 4 summarizes some of the properties of these storms. In the 2020–2021 storms in the STB, and in the 1979 storm in the SSTB, the convective activity partially separated the cyclone into two sides that later reorganized in turbulent patterns whose evolution lasted months (in the STB) or days-weeks (in the SSTB). The 2018 STB storm originated in an elongated cyclone, also producing a complex phenomenology that may have broken the original cyclone in two and resulted in a largely turbulent segment of the STB (Iñurrigarro et al., 2020). The 2020–2021 storms occurred in small cyclones without strong

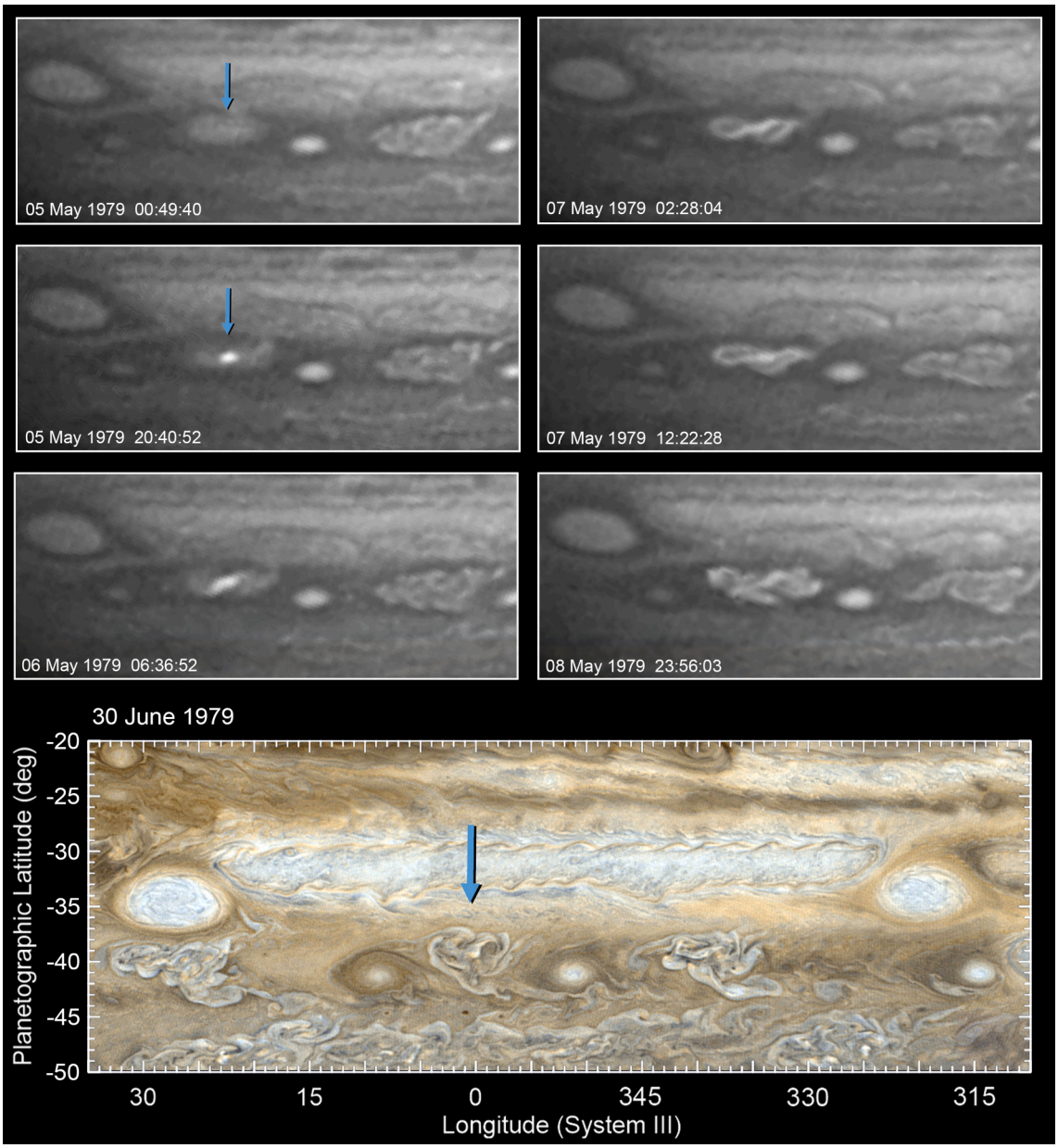

Fig. 19. Voyager 2 images of a convective outbreak at 38.8°S. The lower panel is a high-pass filtered and contrast enhanced version of a true colour map of Jupiter, showing the resulting FFR in the following month. The full map is available at https://bjj.mmedia.is/data/jupiter/index.html

confining boundaries, so, the turbulent region formed appears capable of expanding for a long time, as it has been observed for similar STB segments in the past (Rogers et al., 2013).

The cyclonic circulation in the STB Ghost was about 80 ms^{-1}, whereas in the cyclone where Clyde's Spot developed in 2020 and in the 1979 SSTB cyclone motions seemed much smaller with values about 30–40 ms^{-1}. The numerical simulations of the 2018 storm presented by Iñurrigarro et al. (2020) explored the interaction of convection with the intense circulation of the STB Ghost, but a completely different outcome is expected in the weak circulations of the small STB cyclones studied here. We show in paper 2 that the particular morphologies observed in Clyde's Spot, the 2021 STB storm and the 1979 SSTB storm require an equilibrium between the cyclonic circulation and the intensity of convection powering the storm.

The long-term evolution of the Clyde's Spot and the 2021 STB storm are complex. Both seem affected by the interactions of the disturbed cyclone with the environment, with clear changes in latitude and interactions with other features. In the long-term, one of these storms evolved expanding and forming a structured turbulent sector of the STB, while the other stopped its growth and became a stable dark cyclone of the STB. It is unclear from the limited data around the 2021 STB storm why two storms that shared so many characteristics at their onset and early evolution would diverge so much in their later developments.

Turbulent sectors of the STB have repeatedly arisen east of Oval BA since 2000, usually or always with the evolution of initially small dark cyclonic spots like DS7, which then expanded longitudinally (Rogers et al., 2013; Rogers and Adamoli, 2015). In some cases, STB segments became dark turbulent segments, but previous observations of these events did not have the combination of high-resolution observations and temporal sampling available for Clyde's Spot and the evolution of its remnant, and short-lived convective outbreaks may have passed unnoticed many times in the past. Here, we have observed the formation of an STB segment in intimate detail after the development of a short-lived convective disturbance. In this case, it began as a small, low-contrast cyclone; then a single convective plume erupted within it forming 'Clyde's Spot'. Within a few days the cyclone became a dark spot similar

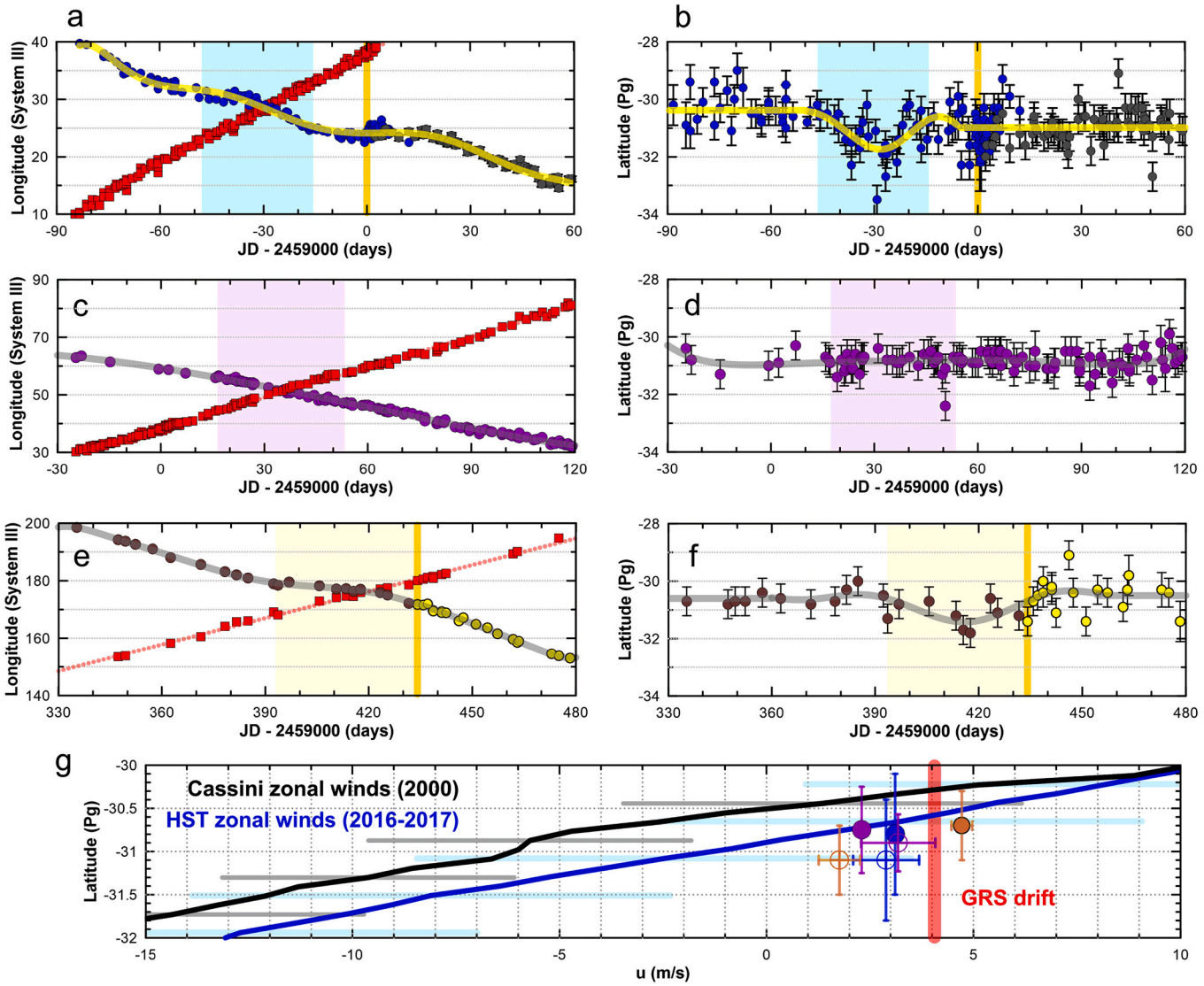

Fig. 20. Interaction of STB cyclones with the GRS. (a) Longitudinal tracking of Clyde's Spot precursor (blue circles) and its outcome as DS7 (black circles) compared with the GRS (red). Shaded area shows the dates of the interaction between both vortices. A vertical yellow line marks the date of the convective outbreak. Polynomial fits to the data are also shown. (b) Same as (a) but for latitudes. (c-d) Same as (a-b) but for DS6 (purple circles). (e-f) Same as (a-b) but for the 2021 STB storm (yellow circles) and its cyclone precursor (brown circles). Symbols follow the same colour convention used in Figs. 15 and 18. (g) Comparison of the drift rate of the different cyclones before reaching the GRS (filled circles, blue for Clyde's Spot, purple for DS6 and brown for the 2021 STB storm) and during their interaction (open symbols) with the zonal winds with their error bars, and the drift rate of the projection of the GRS at the latitude of the cyclones. Cassini zonal winds are from Porco et al. (2003). HST zonal winds are from Hueso et al. (2017). (For interpretation of the references to colour in this figure legend, the reader is referred to the web version of this article.)

to those observed at the initiation of previous STB segments. In this case, we have observed the turbulent nature of this dark spot that gradually expanded until it became a FFR, a precursor of a turbulent STB segment. The combination of visible and infrared images of the FFR phase shows the simultaneous presence of bright clouds and dark clearings in the visible accompanied by dark and bright emissions in the thermal infrared. These structures are compatible with the presence of active cloud formation and small intensity convection during this phase.

In addition, dark cyclones in the STB can be originated as convective storms that do not grow to a large enough size to produce the full phenomenology observed around Clyde's Spot.

9. Summary and conclusions

The combination of Junocam, HST, amateur and other ground-based observations of two small-scale short-lived storms that developed in small cyclones in Jupiter's STB in 2020 and 2021 shows part of the complex meteorology of convective events in gas giants. We here provide a summary of the results of the analysis of the observations of these storms.

Regarding the observations of convective storms in closed cyclones we conclude that:

- The 2020 STB storm known as Clyde's Spot originated in a small-scale cyclone that was the result of the merger of two smaller cyclones months before developing convection. The 2021 STB storm originated in a very similar cyclone that was possibly the outcome of the merger of previous cyclones in the STB. Both cyclones interacted with the GRS days before the start of moist convection within the cyclones. However, the effects of those interactions, and how they could trigger moist convection in the cyclones are unclear.

Table 4
Summary of storms in cyclones in this study compared with similar events.

Storm	Date	Latitude	Vortex size *E*-W (km) N-S (km)	Storm size* E-W (km) N-S (km)	General properties
1979 SSTB	May 1979	−38.8 ± 0.2°	8100 ± 1000 4100 ± 750	(1) 1600 ± 200 1600 ± 300	Compact pulse. Double-lobe structure at peak activity. Bright clouds. Estimated outer velocities in the cyclone: 30 ms^{-1}. No expansion beyond the original cyclone.
2018 STB Ghost	Feb. 2018	−28.0 ± 0.5°	23,000 ± 600 4800 ± 600	No compact storms, elongated clouds.	Two or more pulses. Elongated structures. Bright clouds and dark clearings. Estimated outer velocities in the cyclone: 80 ms^{-1}. Complex evolution of the cyclone after the storm activity.
Clyde's Spot	May 2020	−30.8 ± 0.3°	2200 ± 250 1500 ± 250	(2) 4600 ± 300 2700 ± 200	Previous interaction with the GRS. Compact pulse on a vortex bright in UV. Double-lobe structure at peak activity. Bright clouds and dark clearings. Estimated outer velocities in the cyclone: 30–40 ms^{-1}. Complex long-term evolution with formation of a FFR and a turbulent segment of the STB.
2021 STB	Aug. 2021	−30.3 ± 0.5°	1800 ± 600 1400 ± 600	(3) 3700 ± 600 2200 ± 500	Previous interaction with the GRS. Compact pulse. Double-lobe structure at peak activity. Long-term evolution.

(*) The sizes of the storms are given at their peak with a compact morphology. This is 20 h for Voyager data (1), and 3 days after outbreaks in Clyde's Spot using Junocam data (2) and 3 days after outbreak in the 2021 STB storm using amateur data (3). In the latter two cases this corresponds to the double-lobe morphology.

- In both cases, a convective storm formed inside a small circular cyclone. The storm disrupted the cyclone forming an elevated double-sided structure on time-scales of one to a few days. This behavior is shared with the convective eruption of the SSTB observed by Voyager 2 in 1979. In the case of Clyde's Spot, details of this phase are provided by Junocam and HST images suggesting weak horizontal motions with velocities of about 30–40 ms^{-1} days after the initial explosive outburst of convection. The August 2021 convective outbreak in the STB replicates the details of the activity observed one year earlier in Clyde's Spot with only minor differences. In the three cases, Clyde's Spot, the August 2021 STB storm and the 1979 storm in the SSTB, as well as in the larger storms occurring in the STB Ghost in 2018, the circulation in the cyclone confined the convective activity inside the original cyclones, and bright clouds did not expanded outside of the initial cyclone.
- After the fast outburst that formed Clyde's Spot in May 2020 stopped, the region evolved in a few days to form a dark feature that showed interactions with its environment and changes in latitude and drift rate. This feature later evolved by expanding in both longitude and latitude over the course of about one year forming a FFR-like structure that later grew into an extended turbulent segment of the STB. In these evolved phases, the highest-resolution UV and methane-band images show bright filaments suggestive of strong vertical motions and convection in these highly evolved phases of the cyclonic feature. The high-resolution Junocam images and thermal infrared images from ground-based telescopes show dark clearings and compact clouds coexisting in this large cyclonic system and supporting some degree of vertical convection at a much smaller rate than in the explosive initial outburst. The FFR-like morphology of the evolved phases of Clyde's Spot are very similar to the formation of a FFR in the SSTB observed by Voyager 2. However, both FFRs formed on very different time-scales, with several months in the STB compared with about 10 days in the SSTB. The convective FFR observed by Voyager 2 did not grow in size beyond the original cyclone.
- The expansion rates of clouds associated with Clyde's Spot during its outburst in May–June 2020 was accompanied by high cloud tops. The slow expansion rate of the associated FFR over 2021 was accompanied by low cloud tops on average but with some bright filaments on HST images showing much less energetic convection consistent with to water condensation being the source of the initial outburst and ammonia condensation as the source of the later long-term evolution.
- The complex phenomenology of Clyde's Spot was replicated one year later by the formation of a new storm in a cyclone of the STB also after a similar interaction with the GRS. This storm developed turbulence and dark features just as Clyde's Spot, but it did not achieve the same level of activity and developed into a closed dark cyclone in a time-scale of a few months.

Regarding other aspects of cyclones and the STB:

- Cyclones in the STB form regularly and can have very different properties with varied phases in their complex evolution. A cyclone similar to the precursor to Clyde's Spot observed in 2019, and possibly also formed from the merge of two previously existing cyclones, evolved from its low-contrast initial aspect to form a very dark feature, Dark Spot 6 (DS6), with no observed signs of convection. However, its similarity with the dark cyclone formed in the evolution of the 2021 STB storm, and the long time window in which DS6 was not observed would allow a similar origin. The cyclone later interacted with Oval BA, changing into an orange pale cyclone surrounded by a white annulus and became White Spot 6 (WS6). This cyclone interacted with Oval BA without apparent changes in size or colour and is currently moving away from Oval BA after a small northward migration. The transformations of morphology and colour of this cyclone in the visible were also accompanied by changes in its visibility in thermal infrared images. It was not observable in thermal infrared images in 2019, when it was a low contrast cyclone in the visible. It was very bright in the thermal infrared in 2020, when it was dark-red in the visible (DS6). It was not observable in thermal infrared images in 2021, when it transformed into a brighter cyclone in the visible (WS6).
- Oval BA is also interacting with a very long turbulent segment of the STB in its west flank. This turbulent segment represents the long-term evolution of the cyclonic outcome of the convective storm that originated in 2018 in the STB Ghost.

Outstanding questions on the study of moist convective storms in

Jupiter are how is convection initiated at depth and what is the cycle of activity in different locations of the planet. For instance, how often do storms like these form, and whether they also form at other latitudes that are rich in FFRs. The current exploration of Jupiter by the Juno mission and the extensive survey of its atmosphere that can be done with the combination of amateur and professional observations allows the study of the details of convective storms that would have passed unnoticed in past decades. These storms have complex evolutions and seem to have an important role in the formation of FFRs and other eddies in the bands and belts.

In a companion paper (paper 2), we present our numerical simulations of Clyde's Spot, the August 2021 STB storm and the storm in the SSTB observed by Voyager 2. We study the energetics associated with these storms showing that structures formed in moist convective storms in closed cyclones depend on an equilibrium between the intensity of the circulation in the cyclone and the intensity of the convective power released. In addition, our simulations suggest that the merger of previously existing cyclones was not a driver of convection.

Data availability

All the amateur images used in this paper are available at the PVOL2: http://pvol2.ehu.eus and ALPO-Japan websites: http://alpo-j.sakura.ne.jp/indexE.htm. JunoCam raw images are available at the PDS web site: https://pds-imaging.jpl.nasa.gov/portal/juno_mission.html. Processed versions of these images are available at the MissionJuno web site: https://www.missionjuno.swri.edu/junocam/. Navigated versions produced by G. Eichstädt, are available at: http://junocam.pictures/gerald/uploads/uploads_by_pj.html. Cylindrical maps of JunoCam images are also available at the PVOL2 website at http://pvol2.ehu.eus/. HST images are available at https://archive.stsci.edu/. Mapped versions of HST/OPAL images are available at: https://archive.stsci.edu/prepds/opal/. PlanetCam images during the current study are available from the corresponding author on reasonable request. IRTF images are available at the Juno IRTF open archive at https://junoirtf.space.swri.edu/ and at the NASA/IPAC Infrared Science Archive at https://irsa.ipac.caltech.edu/. Gemini images are available at: https://archive.gemini.edu/. The PICV software can be downloaded from Zenodo with doi: https://doi.org/10.5281/zenodo.4312675.

Declaration of Competing Interest

None.

Acknowledgements

We are very thankful to the large community of amateur observers operating small telescopes that submit their Jupiter observations to databases such as PVOL and ALPO-Japan. We are also grateful to two anonymous reviewers for their comments that improved the clarity of this paper. This work has been supported by Grant PID2019-109467GB-I00 funded by MCIN/AEI/10.13039/501100011033/ and by Grupos Gobierno Vasco IT1366-19. PI acknowledges a PhD scholarship from Gobierno Vasco. GSO and TM were supported by NASA with funds distributed to the Jet Propulsion Laboratory, California Institute of Technology under contract 80NM0018D0004. C. J. Hansen was supported by funds from NASA, USA to the Juno mission via the Planetary Science Institute. IOE was supported by a contract funded by Europlanet 2024 RI to navigate Junocam images, now available as maps in PVOL at http://pvol2.ehu.eus. Europlanet 2024 RI has received funding from the European Union's Horizon 2020 research and innovation programme under grant agreement No 871149. G.S. Orton, S. R. Brueshaber, T. W. Momary, K. H. Baines and E. K. Dahl were visiting Astronomers at the Infrared Telescope Facility, which is operated by the University of Hawaii under contract 80HQTR19D0030 with the National Aeronautics and Space Administration. In addition, support from NASA Juno Participating Scientist award 80NSSC19K1265 was provided to M.H. Wong. This work has used data acquired from the NASA/ESA Hubble Space Telescope (HST), which is operated by the Association of 807 Universities for Research in Astronomy, Inc., under NASA contract NAS 5-26555. These HST observations are associated with several HST observing programs: GO/DD 14661 (PI: M.H. Wong), GO/DD 15665 (PI: I. de Pater), GO/DD 15159 (PI: M. H. Wong), GO/DD 15502 (PI: A. Simon), GO/DD 14661 (PI: M. H. Wong), GO/DD 16074 (PI: M.H. Wong), GO/DD 16053 (PI: I. de Pater), GO/DD 15929 (PI: A. Simon), GO/DD 16269 (PI: A. Simon). PlanetCam observations were collected at the Centro Astronómico Hispánico en Andalucía (CAHA), operated jointly by the Instituto de Astrofisica de Andalucia (CSIC) and the Andalusian Universities (Junta de Andalucía). This work was enabled by the location of the IRTF and Gemini North telescopes within the Maunakea Science Reserve, adjacent to the summit of Maunakea. We are grateful for the privilege of observing Ka'āwela (Jupiter) from a place that is unique in both its astronomical quality and its cultural significance. This research has made use of the USGS Integrated Software for Imagers and Spectrometers (ISIS). Voyager 2 images were accessed through The PDS Ring-Moon Systems Node's OPUS search service.

Appendix A. Supplementary data

Supplementary data to this article can be found online at https://doi.org/10.1016/j.icarus.2022.114994.

References

Barrado-Izagirre, N., Legarreta, J., Sánchez-Lavega, A., Pérez-Hoyos, S., Hueso, R., Iñurrigarro, P., Rojas, J.F., Mendikoa, I., Ordoñez-Etxeberria, I., 2021. Jupiter's third largest and longest-lived oval: color changes and dynamics. Icarus 361, 114394. https://doi.org/10.1016/j.icarus.2021.114394.

Becker, H.N., Alexander, J.W., Atreya, S.K., Bolton, S.J., Brennan, M.J., Brown, S.T., Guillaume, A., Guillot, T., Ingersoll, A.P., Levin, S.M., Lunine, J.I., Aglyamov, Y.S., Steffes, P.G., 2020. Small lightning flashes from shallow electrical storms on Jupiter. Nature 584, 55–58. https://doi.org/10.1038/s41586-020-2532-1.

de Pater, I., 17 colleagues, 2019. First ALMA millimeter-wavelength maps of Jupiter, with a multiwavelength study of convection. Astron. J. 158 https://doi.org/10.3847/1538-3881/ab3643.

Dowling, T.E., 1995. Dynamics of Jovian atmospheres. Annu. Rev. Fluid Mech. 27 (1), 293–334. https://doi.org/10.1146/annurev.fl.27.010195.001453.

Dowling, T.E., Gierasch, P.J., 1989. Cyclones and moist convection on Jovian planets. Bull. Am. Astron. Soc. 21, 946.

Dowling, T.E., Fischer, A.S., Gierasch, P.J., Harrington, J., LeBeau, R.P., Santori, C.M., 1998. The explicit planetary isentropic-coordinate (EPIC) atmospheric model. Icarus 132, 221–238. https://doi.org/10.1006/icar.1998.5917.

Fletcher, L.N., Rogers, J.H., 2018. Pro-am collaborations improve views of Jupiter. Astron. Geophys. 59, 4.24–4.31. https://doi.org/10.1093/astrogeo/aty192.

Fletcher, L.N., Orton, G.S., Rogers, J.H., Giles, R.S., Payne, A.V., Irwin, P.G.J., Vedovato, M., 2017. Moist convection and the 2010-2011 revival of Jupiter's South Equatorial Belt. Icarus 286, 94–117. https://doi.org/10.1016/j.icarus.2017.01.001.

Foster, C., Rogers, J., Mizumoto, S., Orton, G., Hansen, C., Momary, T., Casely, A., 2020. A rare methane-bright outbreak in Jupiter's South Temperate domain. In: 14th Europlanet Science Congress 2020 id. EPSC2020-196.

Hansen, C.J., Caplinger, M.A., Ingersoll, A., Ravine, M.A., Jensen, E., Bolton, S., Orton, G., 2017. Junocam: Juno's outreach camera. Space Sci. Rev. 213, 475–506.

Hueso, R., Sánchez-Lavega, A., Guillot, T., 2002. A model for large-scale convective storms in Jupiter. J. Geophys. Res. Planet 107, 5075. https://doi.org/10.1029/2001JE001839. E10.

Hueso, R., Legarreta, J., García-Melendo, E., Sánchez-Lavega, A., Pérez-Hoyos, S., 2009. The Jovian anticyclone BA: II. Circulation and interaction with the zonal jets. Icarus 203, 499–515. https://doi.org/10.1016/j.icarus.2009.05.004.

Hueso, R., Sánchez-Lavega, A., Iñurrigarro, P., Rojas, J.F., Pérez-Hoyos, S., Mendikoa, I., Gómez-Forrellad, J.M., Go, C., Peach, D., Colas, F., Vedovato, M., 2017. Jupiter cloud morphology and zonal winds from ground-based observations before and during Juno's first perijove. Geophys. Res. Lett. 44, 4669–4678. https://doi.org/10.1002/2017GL073444.

Hueso, R., Juaristi, J., Legarreta, J., Sánchez-Lavega, A., Rojas, J.F., Erard, S., Cecconi, B., Le Sidaner, P., 2018. The planetary virtual observatory and laboratory (PVOL) and its integration into the virtual European solar and planetary access (VESPA). Planet. Space Sci. 150, 22–35. https://doi.org/10.1016/j.pss.2017.03.014.

Hunt, G.E., Müller, J.P., Gee, P., 1982. Convective growth rates of equatorial features in the jovian atmosphere. Nature 295, 491–494. https://doi.org/10.1016/0019-1035(76)90064-6.

Ingersoll, A.P., 8 colleagues, 2004. Dynamics of Jupiter's atmosphere. In: Bagenal, Fran, Dowling, Timothy E., McKinnon, William B. (Eds.), Jupiter. The planet, Satellites

and Magnetosphere, vol. 1. Cambridge University Press, Cambridge, UK, pp. 105–128. Cambridge planetary science. ISBN 0–521–81808-7, 2004.

Iñurrigarro, P., Hueso, R., Legarreta, J., Sánchez-Lavega, A., Eischtädt, G., Rogers, J.H., Orton, G.S., Hansen, C.J., Pérez-Hoyos, S., Rojas, J.F., Gómez-Forrellad, J.M., 2020. Observations and numerical modelling of a convective disturbance in a large-scale cyclone in Jupiter's South Temperate Belt. Icarus 336, 113475. https://doi.org/10.1016/j.icarus.2019.113475.

Iñurrigarro, P., Hueso, R., Sánchez-Lavega, A., Legarreta, J., 2022. Convective Storms in Jupiter's South Temperate Belt Cyclones: (II): Numerical Modelling (in preparation).

Li, L., Ingersoll, A.P., Vasavada, A.R., Porco, C.C., Del Genio, A.D., Ewald, S.P., 2004. Life cycles of spots on Jupiter from Cassini images. Icarus 172, 9–23. https://doi.org/10.1016/j.icarus.2003.10.015.

Lindal, G.F., Wood, G.E., Levy, G.S., Anderson, J.D., Sweetnam, D.N., Hotz, H.B., Buckles, B.J., Holmes, D.P., Doms, P.E., Eshleman, V.R., Tyler, G.L., Croft, T.A., 1981. The atmosphere of Jupiter - an analysis of the Voyager radio occultation measurements. J. Geophys. Res. 86, 8721–8727. https://doi.org/10.1029/JA086iA10p08721.

Little, B., Anger, C.D., Ingersoll, A.P., Vasavada, A.R., Senske, D.A., Brenemen, H.H., Borucki, W.J., the Galileo SSI Team, 1999. Galileo images of lightning on Jupiter. Icarus 142, 306–323. https://doi.org/10.1006/icar.1999.6195.

Mendikoa, I., Pérez-Hoyos, S., Sánchez-Lavega, A., 2012. Probing clouds with a simple radiative transfer model: the Jupiter case. Eur. J. Phys. 33, 1611–1624. https://doi.org/10.1088/0143-0807/33/6/1611.

Mendikoa, I., Sánchez-Lavega, A., Pérez-Hoyos, S., Hueso, R., Rojas, J.F., Aceituno, J., Aceituno, F., Murga, G., De Bilbao, L., García-Melendo, E., 2016. PlanetCam UPV/EHU: a two-channel lucky imaging camera for solar system studies in the spectral range 0.38-1.7 μm. Publ. Astron. Soc. Pac. 128 https://doi.org/10.1088/1538-3873/128/961/035002, 035002.

Mitchell, J.L., Terrile, R.J., Smith, B.A., Muller, J.-P., Ingersoll, A.P., Hunt, G.E., Collins, S.A., Beebe, R.F., 1979. Jovian cloud structure and velocity fields. Nature 280, 776–778. https://doi.org/10.1038/280776a0.

Mousis, O., 59 colleagues, 2014. Instrumental methods for professional and amateur collaborations in planetary astronomy. Exp. Astron. 38, 91–191. https://doi.org/10.1007/s10686-014-9379-0.

Orton, G.S., Hansen, C., Caplinger, M., Ravine, M., Atreya, S., Ingersoll, A.P., Elsa, J., Momary, T., Lipkaman, L., Krysak, D., Zimdar, R., Bolton, S., 2017. The first close-up images of Jupiter's polar regions: results from the Juno mission JunoCam instrument. Geophys. Res. Lett. 44, 4599–4606. https://doi.org/10.1002/2016GL072443.

Pérez-Hoyos, S., Sánchez-Lavega, A., Sanz-Requena, J.F., Barrado-Izagirre, N., Carrión-González, O., Anguiano-Arteaga, A., Irwin, P.G.J., Braude, A.S., 2020. Color and aerosol changes in Jupiter after a north Temperate Belt disturbance. Icarus 352, 114031. https://doi.org/10.1016/j.icarus.2020.114031.

Porco, C.C., West, R.A., McEwen, A., et al., 2003. Cassini imaging of Jupiter's atmosphere, satellites, and rings. Science 299, 1541–1547. https://doi.org/10.1126/science.1079462.

Rayner, J.T., Toomey, D.W., Onaka, P.M., Denault, A.J., Stahlberger, W.E., Vacca, W.D., Cushing, M.C., Wang, S., 2003. SpeX: a medium-resolution 0.8-5.5-micron spectrograph and images for the NASA infrared telescope facility. Pub. Astron. Soc. Pacific. 115, 362. https://doi.org/10.1086/367745.

Reuter, D.C., Simon-Miller, A.A., Lunsford, A., Baines, K.H., Cheng, A.F., Jennings, D.E., Olkin, C.B., Spencer, J.R., Stern, S.A., Weaver, H.A., Young, L.A., 2007. Jupiter cloud composition, stratification, convection, and wave motion: a view from new horizons. Science 318, 223–225. https://doi.org/10.1126/science.1147618.

Rogers, J.H., 2016. Jupiter's South Temperate Domain: Evolution 1991–1999 and Dynamics of Cyclonic Structured Sectors as Seen in Hubble Maps. https://www.britastro.org/node/7230.

Rogers, J., Adamoli, G., 2015. Jupiter's South Temperate Domain, 2012-2015. http://www.britastro.org/jupiter/2014_15report08.htm.

Rogers, J., Adamoli, G., Hahn, G., Jacquesson, M., Vedovato, M., Mettig, H.-J., 2013. Jupiter's South Temperate Domain: Behaviour of Long-Lived Features and Jets, 2001-2012. http://www.britastro.org/jupiter/stemp2013.htm.

Sánchez-Lavega, A., del Río-Gaztelurrutia, T., Hueso, R., Gómez-Forrellad, J.M., Sanz-Requena, J.F., Legarreta, J., García-Melendo, E., Colas, F., Lecacheux, J., Fletcher, L. N., Barrado y Navascués, D., Parker, D., The International Outer Planet Watch (IOPW) Team, 2011. Deep winds beneath Saturn's upper clouds from a seasonal long-lived planetary-scale storm. Nature 475 (7354), 71–74. https://doi.org/10.1038/nature10203.

Sánchez-Lavega, A., Gómez, J.M., Lecacheux, J., Colas, F., Miyazaki, I., Parker, D., Guarro, J., 1996. The South Equatorial Belt of Jupiter, II: the onset and development of the 1993 disturbance. Icarus 121, 18–29. https://doi.org/10.1006/icar.1996.0068.

Sánchez-Lavega, A., Orton, G.S., Hueso, R., García-Melendo, E., Pérez-Hoyos, S., Simon-Miller, A., Rojas, J.F., Gómez, J.M., Yanamandra-Fisher, P., Fletcher, L., Joels, J., Kemerer, J., Hora, J., Karkoschka, E., de Pater, I., Wong, M.H., Marcus, P.S., Pinilla-Alonso, N., Carvalho, F., Go, C., Parker, D., Salway, M., Valimberti, M., Wesley, A., Pujic, Z., 2008. Depth of a strong jovian jet from a planetary-scale disturbance driven by storms. Nature 451, 437–440. https://doi.org/10.1038/nature06533.

Sánchez-Lavega, A., Rogers, J.H., Orton, G.S., García-Melendo, E., Legarreta, J., Colas, F., Dauvergne, J.L., Hueso, R., Rojas, J.F., Pérez-Hoyos, S., Mendikoa, I., Iñurrigarro, P., Momary, T., Hansen, C.J., Eischstaedt, G., Miles, P., Wesley, A., 2017. A planetary-scale disturbance in the most intense Jovian atmospheric Jet from Junocam and ground-based observations. Geophys. Res. Lett. 44, 4679–4686. https://doi.org/10.1002/2017GL073421.

Sánchez-Lavega, A., Hueso, R., Eichstädt, G., Orton, G., Rogers, J., Hansen, C.J., Momary, T., Tabataba-Vakili, F., Bolton, S., 2018. The rich dynamics of Jupiter's great red spot from Junocam: Juno images. Astron. J. 156, 162, 9 pp. https://doi.org/10.3847/1538-3881/aada81.

Sánchez-Lavega, A., Anguiano-Arteaga, A., Iñurrigarro, P., García-Melendo, E., Legarreta, E., Hueso, R., Sanz-Requena, J.F., Pérez-Hoyos, S., Mendikoa, I., Soria, M., Rojas, J.F., Andres-Carcasona, M., Part-Garsull, A., Ordoñez-Etxeberria, I., Rogers, J. H., Foster, C., Mizumoto, S., Casely, A., Hansen, C.J., Orton, G.S., Momary, T., Eischtadt, G., 2021. Jupiter's great red spot: strong interactions with incoming anticyclones in 2019. J. Geophys. Res. Planet 126. https://doi.org/10.1029/2020JE006686 e2020JE006686.

Simon, A.A., Sánchez-Lavega, A., Legarreta, J., Sanz-Requena, J.F., Pérez-Hoyos, S., García-Melendo, E., Carlson, R.W., 2015. Spectral comparison and stability of red regions on Jupiter. J. Geophys. Res. Planet 120, 483–494. https://doi.org/10.1002/2014JE004688.

Smith, B.A., 21 colleagues, 1979. The Galilean satellites and Jupiter: voyager 2 imaging science results. Science 206, 927–950. https://doi.org/10.1126/science.206.4421.927.

Thomson, S.I., McIntyre, M.E., 2016. Jupiter's unearthly jets: a new turbulent model exhibiting statistical steadiness without large-scale dissipation. J. Atmos. Sci. 73 (3) https://doi.org/10.1175/JAS-D-14-0370.1.

Wong, M.H., Simon, A.A., Tollefson, J.W., de Pater, I., Barnett, M.N., Hsu, A.I., Stephens, A.W., Orton, G.S., Fleming, S.W., Goullaud, C., Januszewski, W., Roman, A., Bjoraker, G.L., Atreya, S.K., Adriani, A., Fletcher, L.N., 2020. High-resolution UV/optical/IR imaging of Jupiter in 2016–2019. Astrophys. J. Suppl. Ser. 247, 58, 25pp. https://doi.org/10.3847/1538-4365/ab775f.